RSC Advances

PAPER

View Article Online
View Journal | View Issue

Cite this: *RSC Adv.*, 2026, **16**, 28376

Oxovanadium(IV/V) lawsone-based complexes: synthesis, characterization, DFT studies, and multifunctional biological activities

Islam M. Elnabky,[a] Mohamed M. Aboelnga,[*ab] Heba A. Sahyon,[c] Ahmed M. El-Hendawy[a] and Shadia A. Elsayed[*a]

Three oxovanadium(IV/V) complexes with lawsone (HLw) were synthesized, including $[VO(Lw)_2(H_2O)]\cdot H_2O$ (**1**), $[VO(Lw)_2Cl]\cdot H_2O$ (**2**), and $[VO_2(Lw)(bpy)]$ (**3**). They were characterized by CHN elemental analysis, FTIR, ^{1}H NMR, UV-Vis, ESI-MS, magnetic susceptibility, molar conductivity, and thermogravimetric analysis (TGA), and DFT calculations. Spectroscopic results indicated that the ligand acts as a monoanionic bidentate (O, O) donor ligand. In view of the potential of vanadium-based anticancer agents, the interactions of the complexes with biomacromolecules (ctDNA, tRNA, and BSA) were investigated. The complexes exhibited moderate binding affinity toward ctDNA and tRNA (10^4 M^{-1} range), with a preference for tRNA, and binding modes consistent with partial intercalative and/or surface interactions. Protein binding studies suggested a static quenching mechanism with BSA. The *in vitro* cytotoxic activity was evaluated against HeLa (cervical), HepG-2 (hepatocellular), and MCF7 (breast) human cell lines. Complex (**2**) displayed the highest activity and selectivity (selectivity index = 4.89 against HeLa) compared to Cisplatin, while showing lower toxicity toward WI-38 (lung) cells. The complexes also exhibited antioxidant activity (SOD-like $IC_{50} = 10.27 \pm 0.54$ μM), consistent with their redox properties, which may contribute to their observed cytotoxic effects. DFT calculations and molecular docking studies supported experimental findings, revealing favorable electronic properties and stable interactions with biological targets. In addition, preliminary antibacterial and α-amylase inhibitory assays were performed to explore broader bioactivity. Overall, these findings suggest that oxovanadium–lawsone complexes possess promising biological activity and merit further investigation.

Received 18th March 2026
Accepted 18th May 2026

DOI: 10.1039/d6ra02275h

rsc.li/rsc-advances

1 Introduction

Vanadium is a 3d-series transition metal that exhibits multiple oxidation states, with the +4 and +5 states being of particular biological and therapeutic relevance. Extracellularly, vanadium exists mainly as pentavalent vanadate V(V), whereas intracellularly it is predominantly present as tetravalent vanadyl species V(IV). At trace levels, vanadium displays beneficial biological effects; however, elevated concentrations may result in toxicity. Owing to its bio-essential nature and redox activity, vanadium has attracted considerable attention as a non-platinum metal with promising therapeutic potential, including antitumor properties.[1–4]

The ability of vanadium complexes to undergo redox transformations enables effective interactions with biomolecules such as enzymes and DNA, making them attractive candidates for medicinal applications. In particular, their interactions with DNA have been widely explored because of their potential use as novel anticancer agents and as photochemical probes for DNA structure and conformation.[5] Vanadium complexes have shown a wide range of biological effects; in particular, their antibacterial activity has been noted against both Gram-positive and Gram-negative strains.[6] Additionally, their recognized insulin-mimetic properties make them important candidates in diabetes research.[7] Moreover, certain oxovanadium species have exhibited notable anti-inflammatory properties by influencing oxidative stress,[8] along with their extensively researched capabilities as effective antitumor agents.[9]

Hydroxynaphthoquinones of natural origin constitute an important class of bioactive compounds with significant pharmacological properties. Compounds such as lawsone, plumbagin, juglone, and lapachol are among the most well-known examples.[10,11] The biological properties of these molecules are largely related to redox behavior of the naphthoquinone moiety, which contributes to diverse activities such as antibacterial, anti-inflammatory, and anticancer effects.[12,13]

[a]*Chemistry Department, Faculty of Science, Damietta University, New Damietta, Egypt. E-mail: mohamed-aboelnga@du.edu.eg; shadia.elsayed@du.edu.eg*

[b]*King Salman International University, Faculty of Basic Sciences, Ras Sudr46612, South Sinai, Egypt*

[c]*Chemistry Department, Faculty of Science, Kafrelsheikh University, Kafr Elsheikh, Egypt*

Lawsone (2-hydroxy-1,4-naphthoquinone) is a naturally occurring dye extracted from the henna plant (*Lawsonia inermis*). It has attracted considerable interest because of its biological properties and its wide use in biochemical and analytical applications. Lawsone also represents an important precursor in the synthesis of numerous structurally diverse and biologically active compounds. Among hydroxynaphthoquinones, the 1,4-naphthoquinone form is considered the most stable and consequently the most extensively investigated. The naphthoquinone framework, containing two carbonyl oxygen atoms, is largely responsible for its biological effects, including antimicrobial activity and inhibition of cancer cell proliferation.[14] The biological activities of these compounds are mainly associated with the presence of the quinone moiety and its ability to undergo redox transformations in biological environments through one- or two-electron reduction processes, the quinone moiety can be converted into semiquinone or hydroquinone intermediates, which contribute significantly to their pharmacological effects. In addition, lawsone and related quinone derivatives can coordinate with transition-metal (*d*-block) ions, leading to the formation of stable metal complexes that often exhibit enhanced cytotoxic properties and diverse mechanisms of action.[15,16] Copper(II) is the most popular metal for forming complexes with lawsone, and it has shown potential anticancer activity against several cancer cell lines. The molecular mechanism of these copper(II) lawsone complexes involves the regulation of p53, along with pro-apoptotic proteins Bad and Bax, leading to apoptotic cell death through the activation of caspases 3, 8, and 9.[17] Additionally, various copper(II) complexes that include lawsone as a co-ligand in mixed-ligand arrangements have been shown to interact with calf thymus DNA *via* groove binding. These complexes also exhibit enhanced antimicrobial activity compared to the free ligand.[18] Ruthenium-lawsone complexes have demonstrated *in vitro* cytotoxic activity against prostate, breast, and lung cancer cell lines.[18] Furthermore, dinuclear cadmium complexes containing lawsone have shown significant anticancer and antibacterial activities in comparison to the lawsone ligand.[19] Platinum has also been complexed with Mannich bases derived from lawsone, leading to investigations into DNA binding and cleavage, cellular accumulation, and inhibition of topoisomerase II.[20] Silver(I)–lawsone complexes have shown enhanced biomolecular interactions and promising anticancer activity compared to the free ligand, highlighting the important role of metal coordination in modulating biological properties.[21]

However, despite the extensive studies on vanadium complexes and quinone-based ligands separately, reports on oxovanadium complexes incorporating lawsone as a coordinating bioactive ligand and their combined biomolecular and pharmacological evaluation remain limited. Much of the current research concentrates on the ligands independently or on various metal centers, resulting in a lack of insight into how the distinctive redox-active oxovanadium core engages with the naphthoquinone structure to affect biomolecular targeting. Considering the complementary advantages of lawsone and vanadium, the two components were integrated in the present study to construct new oxovanadium complexes.

In this context, the present work reports the synthesis and characterization of a series of oxovanadium(IV/V) complexes with lawsone (**1–3**). The coordination behavior of lawsone and the structural features of the complexes were elucidated using various physicochemical techniques. Their biological potential was further assessed through anticancer studies against several human cancer cell lines, in addition to evaluating their antioxidant, antibacterial, and α-amylase inhibitory activities. Moreover, density functional theory (DFT) calculations combined with molecular docking simulation were performed to provide insight into the electronic characteristics, chemical reactivity, and possible interactions of the complexes with biological targets. These theoretical approaches provide molecular-level insight into structure–activity relationships and help rationalize their observed biological behavior toward serum albumin and α-amylase. This integrated approach aims to establish structure–activity relationships and to highlight vanadium-lawsone complexes as promising multifunctional candidates for further development in medicinal applications.

2 Experimental

2.1 Materials and methods

The precursors $VOCl_3$, lawsone, bipyridine and phenanthroline were purchased from Alfa Aesar; deoxyribonucleic acid calf thymus (CT DNA, Type XV), 3-(4,5-dimethylthiazol-2-yl)-2,5-diphenyltetrazolium bromide (MTT), and DMEM were procured from Sigma, while the bovine serum albumin (BSA, 98.5%) was obtained from Biomark. Fetal Bovine serum was obtained from GIBCO, UK. All solvents (HPLC grade) and materials were used as received. The cell lines, the normal human lung cells (WI38), Liver cancer cells HePG-2, breast cancer (MCF7), and human cervical carcinoma (HeLa) were obtained from ATCC (Cairo, Egypt).

Fourier-transform Infrared spectra (FTIR, KBr pellets, 4000–400 cm^{-1}) were recorded on a JASCO FT/IR-4100 spectrometer. The NMR spectra was measured on Bruker 400 in DMSO-d6. Electronic spectra of the compounds (2.5×10^{-5} M in DMSO solvent) were measured in the range of 200–900 nm using a JASCO V-630 double-beam spectrophotometer. Fluorescence spectra measurements were carried out on HASCO FP-8350 spectrofluorometer. HRES-MS Bruker compact LC-QTOF/HRMS, Bruker Daltonik Gmbh, Germany. Thermal Gravimetric Analyses data (TGA) were collected in the temperature range 20–800 °C under nitrogen atmosphere of 15.00 mL min^{-1} using Shimadzu TGA-50 Instrument at heating rate of 20 °C min^{-1}. Elemental analyses was performed by PerkinElmer Series II CHNS/O analyzer. Molar conductance values were measured using a 10^{-3} M solution of complexes in DMSO using CM-1K portable conduct meter. Magnetic susceptibility was measured using Sherwood Scientific magnetic susceptibility balance (on powdered samples at room temperature). The thermometer melting point apparatus (RUMO 4000) was used to measure the melting points of the compounds.

2.2 Synthesis of V(IV)/(V) lawsone complexes

2.2.1 $[VO(Lw)_2(H_2O)]\cdot H_2O$ (1). This complex has been prepared with modification of the early reported method,[22] briefly, a $[VO(acac)_2]$ (0.25 mmol, 0.07 g) in 10 mL ethanol was mixed with 5 mL of HLw (0.5 mmol, 0.09 g). The reaction mixture was refluxed while stirring for three hours. The dark brown solution was evaporated under N_2 till near dryness. An excess amount of diethyl ether was then added, yielding a brown precipitate. This precipitate was washed with diethyl ether then dried under vacuum. Yield: 55%. M.p. 238–240 °C (decomposed). Elemental analysis: Calc. for $C_{20}H_{14}O_9V$: C, 53.47; H, 3.14%, found: C, 53.14; H, 3.0., FTIR (KBr, ν cm^{-1}): $\nu(C_4{=}O)$ 1662, $\nu(C_1{=}O)$ 1586, ν(C–O) 1267, ν(VO) 986, ν(V–O) 493. UV-Vis (in DMSO, 2.5 $\times$ 10^{-5} M): λ_{nm} (ε, M^{-1}, cm^{-1}): 267 (2.49 $\times$ 10^4). Molar conductivity (Λ_m, 8.0 S m^2 mol^{-1}). Magnetic moment (μ_{eff} 1.72 B.M.).

2.2.2 $[VO(Lw)_2Cl]\cdot H_2O$ (2). Vanadium oxychloride ($VOCl_3$, 0.5 mmol, 50 μL, 0.09 g) was dissolved in 3 mL of CH_2Cl_2. Separately, HLw (1.0 mmol, 0.18 g) was dissolved in 5 mL of CH_2Cl_2 and then added dropwise to the vanadium solution, resulting in an immediate violet-colored solution. The mixture was stirred at room temperature for 4 h. Subsequently, the solution was concentrated to approximately one-third of its original volume, and a brown precipitate formed upon addition of excess diethyl ether. The resulting product was collected by filtration, washed with diethyl ether, and dried under vacuum. Yield: 65%. M.p. 149–151 °C (decomposed). Elemental Anal. Calc. for $C_{20}H_{10}ClO_7V$: C, 53.54; H, 2.25%, found: C, 53.21; H, 2.12. FTIR (KBr, ν cm^{-1}): $\nu(C_4{=}O)$ 1643, $\nu(C_1{=}O)$ 1579, ν(C–O) 1267, ν(V=O) 994, ν(V–O) 505 cm^{-1}. ^{1}H NMR (500 MHz, DMSO-d_6): Lw signals, δ, ppm = 6.15 (H (3) s, 1H); 7.94 (H(5,8) d, 2H); 7.81 (H(6,7) t, 2H); ESI-MS (m/z): 448.01 (Calcd 447.95). UV-Vis (in DMSO, 2.5 $\times$ 10^{-5} M): λ_{nm} (ε, M^{-1}, cm^{-1}): 270 (3.02 $\times$ 10^4). Molar conductivity (Λ_m, 12.0 S m^2 mol^{-1}). Magnetic moment (μ_{eff} 0 B.M., diamagnetic).

2.2.3 $[VO_2(Lw)(bpy)]$ (3). A methanolic solution (5 mL) of HLw (0.5 mmol, 0.09 g) was mixed with methanolic solution (5 mL) of bpy (0.5 mmol, 0.08 g) and heated under reflux for an hour. Then, an aqueous methanolic solution of NH_4VO_3 (0.5 mmol, 0.06 g) dissolved in 15 mL (1 : 2 v/v H_2O to CH_3OH) was added and refluxed for another three hours to obtain an orange precipitate. The orange product was filtered off, washed with diethyl ether, and dried in *vacuo*. Yield: 58%. M.p. 240–242 °C (decomposed). Elemental Anal. Calc. for $C_{20}H_{13}N_2VO_5$: C, 58.27; H, 3.18; N, 6.79%, found: C, 58.01; H, 3.11; N, 6.46%. FTIR (KBr, cm^{-1}): $\nu(C_4{=}O)$ 1640, $\nu(C_1{=}O)$ 1595, ν(C=N) 1558, ν(C–O) 1264, ν(VO)/VO_2 933, 900, ν(V–O) 494. ^{1}H NMR (500 MHz, DMSO-d_6): Lw signals, δ, ppm = 6.22 (H(3), s, 1H); 7.46 (H (5) d, 1H); 7.66 (H(8) d, 1H); 7.85 (H(6,7), t, 2H) bpy signals: δ ppm = 7.97 (t, 4H); 8.40 (d, 2H); 8.7 (d, 2H). ; ESI-MS (m/z): 413.04 (Calc. 412.02). UV-Vis (2.5 $\times$ 10^{-5} M, DMSO, λ_{nm} (ε, M^{-1}, cm^{-1}): 270 (4.03 $\times$ 10^4). Molar conductivity (Λ_m, 3.8 S m^2 mol^{-1}). Magnetic moment (μ_{eff} 0 B.M., diamagnetic).

2.3 Biological evaluation assays

To evaluate the biological relevance of the complexes, detailed nucleic acid and protein binding studies were performed, followed by cytotoxic evaluation. Additional antioxidant, antibacterial, and α-amylase inhibition assays were conducted as preliminary screening to explore broader bioactivity.

2.3.1 Interaction with ctDNA/tRNA and BSA

2.3.1.1 Absorption studies. The ctDNA, tRNA, and BSA binding studies were implemented according to literature procedures.[23] Electronic absorption titration experiments were performed using a fixed concentration of the vanadium complexes (50 μM) in a DMSO/Tris–HCl buffer system, while gradually increasing the concentration of ctDNA (0–100 μM) in 5 mM Tris–HCl/50 mM NaCl buffer at pH 7.2, following previously reported procedures. The purity of ctDNA was confirmed by the absorbance ratio at 260/280 nm, which was found to be 1.9, confirming the absence of protein contamination. The concentrations of ctDNA and tRNA (per nucleotide) were determined using their molar extinction coefficients at 260 nm (ε = 6600 M^{-1} cm^{-1} for CT-DNA and ε = 7700 M^{-1} cm^{-1} for tRNA). The absorption spectra were recorded over the range of 250–600 nm. To eliminate the intrinsic absorbance of the nucleic acids, equal amounts of CT-DNA were added to both the reference and sample cuvettes.

The interaction of BSA with the compounds was also studied by absorption spectra using a fixed amount of BSA (50 μM) with addition of incremental amounts of the test compounds (0–100 μM). The electronic spectra were collected in the spectral range of 250–400 nm.

2.3.1.2 Fluorescence studies. Fluorescence spectroscopy was employed to further examine the interaction of the complexes with nucleic acids and protein. Competitive binding studies were carried out using Ethidium bromide (EB) as a fluorescent probe. Ethidium bromide (EB) displacement assay was employed to investigate the interactions of the ligand and its complexes with ctDNA and tRNA, Fluorescence measurements were recorded using an excitation wavelength of λ_{ex} 320 nm (λ_{em} 595 nm) while emission spectra were monitored in the range of 520–750 nm. A fixed concentration of EB (5 μM) and nucleic acids (100 μM ctDNA/tRNA) was used. The test complexes were added incrementally (0–100 μM) in the cuvette, and the mixtures were incubated for 5 min at room temperature prior to measurements. A fluorescence titration was performed by successive additions of the complexes to the EB–nucleic acid system under constant experimental conditions.

The interaction with BSA was also examined using fluorescence quenching measurements. The intrinsic fluorescence of BSA was monitored at an excitation wavelength of 280 nm and emission around 345 nm using a 50 μM BSA solution in phosphate-buffered saline (pH 7.2). Increasing concentrations of the complexes (0–100 μM) were added, and changes in fluorescence intensity were recorded to evaluate the quenching behavior. The emission spectra were recorded over the range of 200–600 nm.

2.3.2 Anticancer activity. The MTT assay was used to determine and compare the IC_{50} values of the vanadium complexes with those of a standard anti-cancer agent (cisplatin). The cytotoxic properties of complexes (**1–3**), and the ligand were assessed against the MCF-7 (ATCC HTB-22), HeLa (ATCC CCL-2), HepG2 (ATCC HB-8065), and normal human

fetal lung fibroblast (WI38, ATCC CCL-75) cell lines. The cell lines were cultured in RPMI-1640 medium (Gibco™) with 10% fetal bovine serum. This medium was selected to provide essential amino acids, vitamins, and inorganic salts necessary for the sustained growth of these specific adherent cell lines. To the culture medium, antibiotics, penicillin (100 units per mL), and streptomycin (100 μg mL^{-1}) were added. The anticancer effects of these complexes on cancer cell proliferation, *in vitro*, were analyzed using the MTT assay to determine and compare their IC_{50} values with that of the standard anti-cancer agent, cisplatin.[21,24] This colorimetric assay relies on the conversion of yellow tetrazolium bromide (MTT) into a dark blue formazan compound by the mitochondrial enzyme succinate dehydrogenase in living cells. Cells were plated in a 96-well plate and then incubated at 37 °C for 24 hours with 5% CO_2 until reaching a density of 1×10^4 cells/100 μL culture medium for every well. After the incubation period, the cells were treated with various concentrations (100–1.56 μg mL^{-1}) of the complexes and cisplatin dissolved in DMSO and left to incubate for 24 hours; then, 20 μL of MTT solution (5 mg mL^{-1}) was added and incubated for an additional 4 hours. Dimethyl sulfoxide (DMSO) (100 μL) was added to each well to dissolve the formazan, creating purple-colored solutions. Subsequently, colorimetric measurements at 570 nm were recorded. Finally, the IC_{50} values (the concentration required to inhibit 50% of cell growth, determined by SPSS software) were calculated and compared with those of cisplatin. All experiments were conducted in triplicate.

2.3.3 Additional biological screening

2.3.3.1 Antioxidant activity. The SOD-like activity assessed the ability of the tested complexes to scavenge superoxide radicals, which inhibits the color change in the reaction due to the presence of the SOD enzyme or similar compounds.[25] Different concentrations (0.02, 0.04, 0.06, 0.08, 0.1, and 0.2 mg mL^{-1}) of the tested complexes (1, 2, and 3), totaling 0.1 mL, were combined with 0.36 mL of phosphate buffer (0.1 M, pH 8.3), 0.15 mL of nicotinamide adenine dinucleotide (NAD), and 0.15 mL of nitro tetrazolium blue (NBT) at 0.3 mM, followed by the sequential addition of 0.05 mL of phenazine methosulphate (PMS) at 0.93 mM. In the control tube, 0.1 mL of saline was used in place of the samples. The reaction commenced immediately after the addition of PMS, and the change in absorbance at 560 nm was monitored at 0, 1, 2, and 3 minutes until the color change ceased. The inhibition of NBT by the samples was calculated using the following formula:

$$\text{Scavenging activity of NBT}(\%) = \frac{(\text{change in absorbance of blank} - \text{change in absorbance of sample})}{\text{change in absorbance of blank}} \times 100$$

2.3.3.2 α-Amylase inhibition. The antidiabetic effect was assessed by measuring how effectively the tested complexes inhibited α-amylase activity.[26] Various concentrations (0.02, 0.04, 0.06, 0.08, 0.1, and 0.2 mg mL^{-1}) of each complex (0.2 mL) were mixed with 0.1 mL of α-amylase (0.75 U mL^{-1}) and 0.1 mL of starch (1% w/v), and the mixture was allowed to incubate for 3 minutes at 25 °C. After incubation, 0.1 mL color reagent (a combination of DNSA and PSTH) was added to each test tube and then heated for 15 minutes in a boiling water bath. Once the boiling was completed, the tubes were placed in ice to cool down to room temperature. Each tube was subsequently diluted with 0.9 mL of distilled water. The control sample was prepared the same way as the test samples, but distilled water was used in place of the sample. The absorbance for each test tube was measured at 540 nm. To determine the concentration that reduces enzyme activity by 50%, a graphical depiction of the relationship between concentration and inhibition was generated to compute the IC_{50}.

2.3.3.3 Antibacterial activities. The effectiveness of the tested complexes in preventing bacterial growth was evaluated by measuring the diameter of the clear zone in millimeters. Two types of Gram-positive bacteria, *Staphylococcus aureus* (ATCC-6538) (*S. aureus*) and *Bacillus cereus* (ATCC-6633) (*B. cereus*), as well as two Gram-negative bacteria, *Escherichia coli* (ATCC-8739) (*E. coli*) and *Klebsiella pneumoniae* (ATCC-10031) (*K. pneumoniae*), were included in the study.[27] These bacterial strains were cultivated on blood agar for 48 hours at 40 °C and subsequently transferred to neutral agar in appropriate bacterial culture dishes. A volume of 0.01 mL from each complex solution (10 μg complex concentration per disc) was placed on sterile filter paper discs with a diameter of 6 mm, which were then added to the prepared bacterial culture dishes and incubated for 48 hours at 37 °C, following the disk diffusion method.[28] Each plate test was performed in triplicate. The inhibition zones (in mm) were measured using a suitable ruler after the incubation period. An inhibition zone exceeding 10 mm indicates that the substance is deemed active; however, an inhibition zone less than 10 mm indicates resistance.

2.4 Statistical analysis

The experiments were carried out at least three times, and the findings are shown as the mean ± standard error of the mean (SEM). Statistical evaluations were conducted using Minitab 18 software. Results were considered significant if the *P* value was below 0.05.

2.5 Computational studies

2.5.1 DFT studies. The most stable geometries of the investigated complexes were optimized using DFT calculations conducted with the Gaussian09 software package.[29] The B3LYP functional[30–32] was performed together with the 6-31+G(d) basis set for all atoms, while the Vanadium center was treated using the LANL2DZ effective core potential (ECP) basis set. Moreover,

to overcome the limitation of B3LYP and guarantee proper representation for non-covalent interactions and functional, Grimme dispersion correction GD3 was employed.[33] The selected functional and basis set has seen extensive use in describing a range of chemical systems.[34,35]

Frequency calculations were employed at the same theoretical level to validate the optimized structures. The lack of imaginary frequencies ensured that the obtained structures correspond to true minima on the potential energy surface. Furthermore, Gaussian 09 software, together with GaussView, was employed to examine the molecular orbitals, including the highest occupied molecular orbital (HOMO), the lowest unoccupied molecular orbital (LUMO), and the electrostatic potential maps, providing additional understanding into the electronic characteristics of the complexes.

2.5.2 Molecular docking. Molecular docking calculations were conducted using AutoDock4 (ref. 36) to examine the binding interactions between the Vanadium complex and both BSA and amylase receptors. The crystal structures of BSA (PDB ID: 6QS9)[36] and amylase (PDB ID: 5U3A)[37] were obtained from the Protein Data Bank and prepared by eliminating crystallographic water, providing Kollman charges introducing missing hydrogen atoms. Similar docking protocol to our recent articles has been employed in this study.[38] Standard amino acid residues were treated using the default AutoDock force field parameters, and the prepared macromolecules were converted into pdbqt format to incorporate atom types, partial charges, and bond information.

The DFT-optimized Lw and complex (**2**) acted as ligands and were also converted into pdbqt format, with atomic charges assigned using the Gasteiger method. A blind docking approach was adopted by defining a grid box including the receptor structure to permit unbiased determination of possible binding sites. The Lamarckian Genetic Algorithm with 30 independent runs was employed to ensure accurate sampling of conformational space. The most favorable binding pose was selected according to the lowest docking energy, which accounts for electrostatic interactions, van der Waals forces, hydrogen bonding, and desolvation effects. The optimal receptor–ligand complexes were then displayed and analyzed using UCSF Chimera[39] to analyze binding geometry, hydrogen bonding, hydrophobic interactions, and overall structural complementarity.

3 Results and discussion

3.1 Vibrational spectra

The FTIR spectral assignments of vanadium complexes (**1–3**) are stated in the Experimental section (2.1). The ligand (HLw) shows characteristic bands at 3100, 1680, and 1600 cm^{-1} which are assigned to ν(CH), ν(C=O) and ν(C=C) stretches, respectively. The broad band that appeared at 3200 cm^{-1} is due to ν(OH) which is involved in intramolecular hydrogen bond. The presence of [–C=O] shows that the ligand exists in keto–enol form.[16] The region between 1600 and 1680 cm^{-1} displays intense vibrational modes for naphthoquinone ligands, corresponding to the $\nu(C_1{=}O)$ and $\nu(C_4{=}O)$ stretching vibration. Upon the complexation, these bands are shifted into lower frequencies by (5–40) cm^{-1}, and the ν(OH) band disappeared. This indicated that the ligand coordinated to the V(IV)/(V) centers as a mono-negative bidentate O, O-donor. The same behavior was observed in earlier reports.[15,16] The complexes **1** and **2** showed new bands around 986 and 994 cm^{-1}, respectively due to ν(V=O) stretching vibration. However, in complex (**3**), the dioxo groups appeared at 943 and 900 cm^{-1} due to ν_{as} and ν_s *cis*-(VO_2) stretching vibrations.[40,41] In complexes **1** and **2**, the band observed around 3200–3500 cm^{-1} is assigned to the ν(OH) of the crystalline/coordinated water molecules. The characteristic bands of 2,2′-bipyridine are observed at range ~1595, 840 and 725 cm^{-1} which was observed at lower frequency than those of the free bpy,[42] a new medium band at 414 cm^{-1}, assigned to (V–N) stretching, confirms the coordination of bpy to the V(V) center, while the bands at 493–505 cm^{-1} are attributed to ν(V–O) stretching vibrations, confirming the coordination to the lawsone moiety. All The FTIR spectra of the ligand and complexes (**1–3**) are shown in (Fig. S1), and the proposed structure are displayed in Scheme 1.

3.2 ^{1}H NMR spectra

The ^{1}HNMR spectra HLw and its vanadium(V) complexes (**2** and **3**) and their assignments are displayed in Fig. S2a–c), and Experimental section (2.2). As early assigned,[16] the ^{1}H NMR

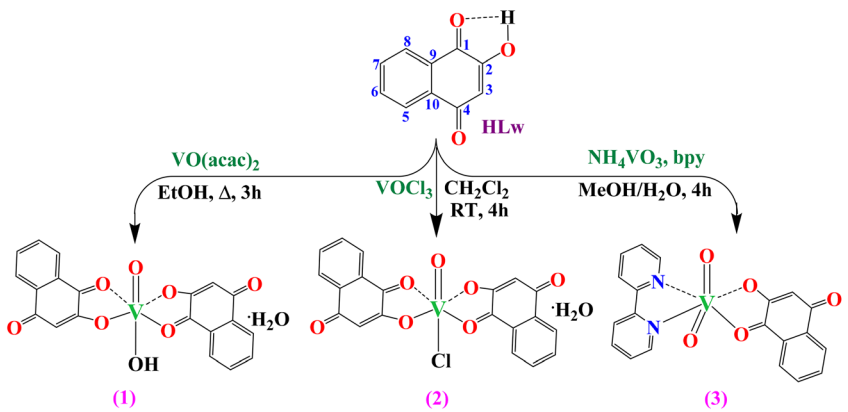

Scheme 1 Synthetic route of vanadium-lawsone complexes (**1–3**).

spectrum of HLw (Fig. S2a) showed a broad signal at δ 11.63 ppm indicative of intramolecular hydrogen bonding, while two triplet of doublets (td) appeared at δ 7.75 and δ 7.79 ppm are ascribed to H6 and H7, respectively. Lastly, the two doublets of doublets (dd) signals at δ 7.89 and δ 7.95 ppm are attributed to H8 and H5, respectively.

In the ^{1}H NMR spectra of complexes (**2, 3**) (Fig. S2b and c), the disappearance of the phenolic hydroxyl proton (2-OH) indicates coordination *via* deprotonation. The H3, H5, and H8 signals experienced downfield shifts relative to the free HLw, reflecting the effect of coordination at neighboring donor sites. For complex **3**, four new resonances at δ 7.97 (t, 4H), 8.40 (d, 2H), and 8.70 (d, 2H) ppm were attributed to the protons of the 2,2′-bipyridine ligand.[43]

3.3 Mass spectra

The ESI-MS spectra of the complexes were recorded in positive ion mode. The spectrum of complex (**1**) (Fig. S3a) exhibited a prominent peak at m/z = 432.19 (calcd 431.0), corresponding to the $[VO(Lw)_2(H_2O)]^+$ molecular ion in agreement with the previously reported structure of the complex.[22] The ESI-MS of the complex **2** $[VO(Lw)_2Cl]$ (Fig. S3b) displayed a base peak at m/z = 448.01 (Calcd 447.95), which corresponds to the $[M]^+$ ion. The second peak was observed at m/z = 411.98 (Calcd 412.98) corresponds to the loss of Cl ligand. The ESI-MS spectrum of $[VO_2(Lw)(bpy)]$ (**3**) (Fig. S3c) shows first fragment at m/z = 411.98 (Calc. 412.02) corresponding to $[M + H]^+$ ion. The second peak in negative ion mode corresponds to the loss of bipyridine unit at m/z 255.98 (Calc. 255.95).

3.4 Electronic spectra and magnetic measurements

The UV-Vis spectra of lawsone and its vanadium complexes were performed in DMSO at 50 μM (Fig. 1). Two absorption bands were observed in the ligand spectrum, at 263 nm (π–π^*) and 280 nm (n–π^*), assigned to intraligand transitions.[16] The electronic spectrum of V(IV) complex (**1**) showed as a slightly red shift of these peaks, 264 and 288, additionally the weak broad peak observed at 486 nm assigned to the d–d transition aligned with d^1 configuration of V(IV) ion. These bands ($^2T_2g \rightarrow {}^2Eg$) are typical for distorted octahedral VO^{2+} complex.[22,44–46] In the electronic spectra of the V(V) complexes, **2** and **3** are like that of the ligand, with slight red of the ligand transition bands coincide with the d^0 configuration of V(V) center. This was further supported by magnetic susceptibility measurements of the solid complexes at 298 K. the complex (**1**) showed paramagnetic behavior with μ_{eff} 1.72 BM which is close to the spin only values,[46] while the complexes (**2** and **3**) showed diamagnetic behavior. The molar conductance of HLw and the complexes was measured in DMSO at a concentration of 1.0×10^{-3} M. The results indicated that all complexes are non-electrolytes, with molar conductance values ranging from 3.8 to 12.0 S m^2 mol^{-1}.

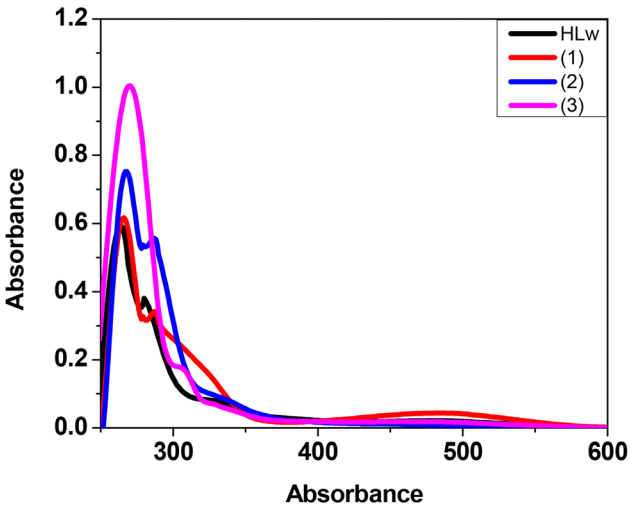

Fig. 1 Electronic spectra of (HLW) and its V(IV/V) complexes in DMSO (2.5×10^{-5} M).

3.5 Thermal analysis

The thermogravimetric diagram of $[VO(Lw)_2(H_2O)]\cdot H_2O$ (**1**) (Fig. S4a) shows three decomposition steps; the first step started from the ambient to 160 °C with weight loss of 7.92% (Calcd 8.0%) corresponds to loss of crystalline and coordinated water molecule. The second stages started in the temperature range 160–420 °C with weight loss of 59.96% (Calcd 59.24%) due to the step wise degradation of the lawsone units ($C_{20}H_{10}O$) fragment. The final step started at 420 °C, leaving a vanadium oxide residue (~32%), likely VO_2 or V_2O_5.

The TGA thermogram of the complex $[VO(Lw)_2Cl]\cdot H_2O$ (**2**) (Fig. S4b) shows different decomposition steps. The initial weight loss observed between 30 and 155 °C corresponds to the loss of one lattice water and Cl ligand with weight loss of 11.11% (Calcd 11.4%). The second weight loss started from 156–360 °C with mass loss of 68.6(67.4%) which is attributed to the thermal degradation of the two organic lawsone ligands. Finally, the final plateau beyond 360 °C indicates the formation of a thermally stable residue likely composed of vanadium oxides accounting for around 21.85% of the initial mass.

The TGA thermogram of $[VO_2(Lw)(bpy)]$ (**3**) (Fig. S4c) shows thermal stability up to 200 °C, this indicates that the complex is free from lattice or coordinated water molecules. The significant mass loss observed between 200 and 455 °C corresponds to the decomposition and volatilization of the bpy and C_9H_5O from lawsone ligand 68.4% (Calcd 69.09%), The thermally stable residue remaining above 600 °C is attributed to vanadium dioxide (VO_2), representing about 20.06% of the original complex mass. The DTG curve supports this assignment, showing a strong, broad peak in the decomposition temperature range. The thermal behavior reflects the robust coordination of the organic ligands and the stability of the VO_2 residue.

3.6 Computational studies

The optimized geometries of the vanadium complexes (**1–3**) (Fig. 2) reveal important structural differences that directly influence their electronic properties and potential biological activity. Complexes **1** and **2** possess very similar coordination environments, differing only in the nature of the axial ligand. In Complex **1**, a water molecule occupies the axial position,

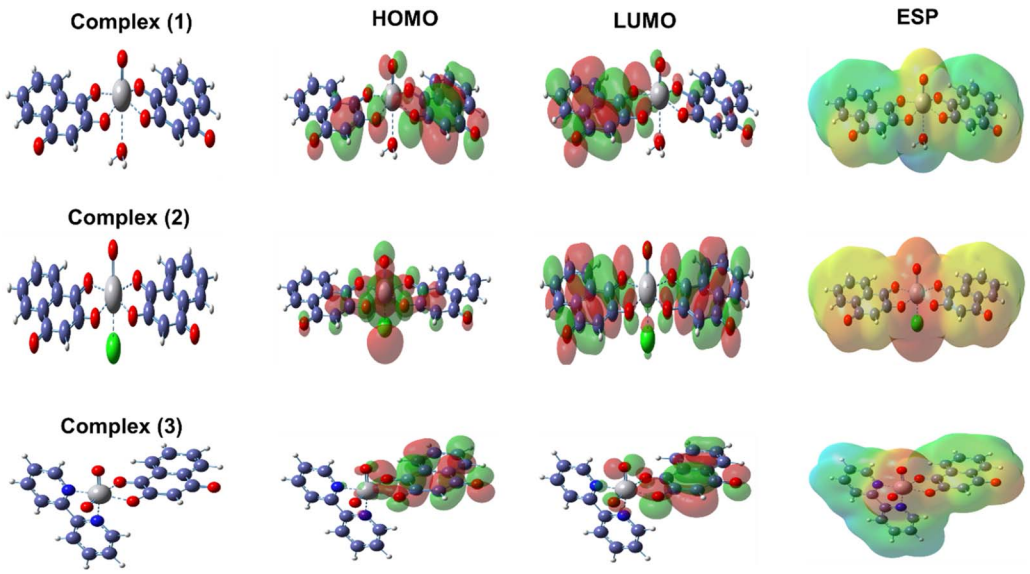

Fig. 2 The optimized molecular structures for the prepared complexes together with their HOMO, LUMO and ESP.

whereas in Complex **2** this position is coordinated by a chloride ion. In both complexes, the vanadium center adopts a distorted octahedral geometry coordinated by two identical deprotonated hydroxynaphthoquinone ligands and one terminal oxo group positioned *trans* to the axial ligand (H_2O or Cl^-). The average V–O bond distances involving the hydroxynaphthoquinone oxygen atoms fall within the range 1.97–2.20 Å, consistent with strong coordination through oxygen donor atoms. In contrast, the vanadium–oxo (V═O) bond length is significantly shorter, approximately 1.59 Å, confirming its multiple-bond character and strong π-interaction. The axial V–Cl bond length (2.48 Å) is shorter than the V–OH_2 bond (2.55 Å), indicating stronger σ-donation from chloride, while the longer V–OH_2 distance suggests greater lability and a higher probability of ligand exchange under physiological conditions.

Complex **3** exhibits a distinctly different coordination pattern. Instead of a mono-oxo environment, it contains a vanadium oxide (dioxo) core coordinated to one deprotonated hydroxynaphthoquinone ligand and one 2,2′-bipyridine (bpy) ligand. The two V═O bonds maintain short distances of approximately 1.59 Å, characteristic of strong multiple bonding. The remaining V–O bond distances lie within the 1.97–2.20 Å range. The presence of the chelating bpy ligand increases the rigidity of the structure and extends the π-conjugation framework, thereby significantly modifying the electronic distribution compared to Complexes **1** and **2**.

Analysis of the frontier molecular orbitals (HOMO and LUMO) provides insight into the electronic behavior of these complexes. In complexes **1** and **2**, the HOMO is predominantly localized over the π-system of the hydroxynaphthoquinone ligands, with partial contribution from vanadium d-orbitals. This indicates that electron donation is largely ligand-centered, facilitating potential π–π interactions with biological macromolecules such as DNA bases or aromatic amino acid residues. The LUMO, on the other hand, is mainly centered on the vanadium atom and the antibonding orbitals of the V═O group, highlighting the electrophilic nature of the metal center. The substitution of water by chloride in complex **2** slightly increases electron density at the metal due to the stronger donor ability of chloride, subtly affecting the orbital distribution and potentially influencing redox behavior and binding affinity.

In complex **3**, the HOMO is more extensively delocalized over both the hydroxynaphthoquinone and bpy ligands, reflecting enhanced conjugation within the coordination sphere. The LUMO remains largely localized on the vanadium oxide moiety, reinforcing its role as the principal electron-accepting site. The increased delocalization and potential reduction in the HOMO–LUMO energy gap suggest higher chemical reactivity for this complex, which may translate into enhanced biological performance.

The electrostatic potential (ESP) maps further clarify the reactivity patterns. Strongly negative regions are concentrated around the oxo oxygen atoms and the phenolic oxygen atoms of the hydroxynaphthoquinone ligands, indicating favorable sites for hydrogen bonding and interactions with positively charged biomolecular residues. Positive electrostatic regions are mainly located around the vanadium center and, in the case of Complex **1**, partially around the hydrogen atoms of the coordinated water molecule. In Complex **2**, the chloride ligand introduces a localized negative electrostatic region along the axial direction, which may influence long-range electrostatic interactions. Complex **3** displays a highly polarized charge distribution due to the presence of two oxo groups and the aromatic bpy ligand, enhancing its capacity for electrostatic attraction toward sitively charged sites in proteins or nucleic acids.

4 Biological applications

This section describes the biological applications of the synthesized complexes.

4.1 CtDNA/RNA binding studies

Interactions with nucleic acids such as DNA and RNA play a crucial role in understanding the biological activity and possible mechanism of action of metal-based complexes. Therefore, the binding behavior of the complexes toward calf thymus DNA (ctDNA) and RNA was investigated using spectroscopic techniques.

4.1.1 Absorption studies. UV-Visible spectra is an essential tool for evaluating the mode of binding of small molecules with biomacromolecules such as DNA, RNA, and BSA. This technique depends on observation of absorption intensity changes demonstrated as either hypochromism or hyperchromism The electronic spectra of V(IV/V) complexes (**1–3**) were recorded both in the absence and presence of various concentrations of ctDNA/tRNA (0–100 μM), while keeping the concentration of the vanadium complexes constant at 50 μM in Tris–HCl buffer (pH 7.2). Upon incremental addition of ctDNA/tRNA to the vanadium (IV/V) complexes, a gradual increase in absorption intensity (hyperchromism) was observed in the regions of 250–300 nm and 400–500 nm (Fig. 3 and 5), with hyperchromic percentage ranging from 31.4% to 60% for ctDNA and 22.9 to 48.0% for tRNA. This phenomenon is changes in the secondary structure of the DNA double helix, likely induced by the interaction with the metal complexes.[45,47] The hyperchromism observed indicates a surface interaction between the positive charges of vanadium (IV/V) complexes and negative charged phosphate backbones of ctDNA/tRNA, predominantly driven by electrostatic forces. To evaluate the binding affinity quantitatively, the intrinsic binding constants (K_b) were determined using the Wolfe–Shimer eqn (1).

$$\frac{[DNA]}{(\varepsilon_a - \varepsilon_f)} = \frac{[DNA]}{(\varepsilon_b - \varepsilon_f)} + \frac{1}{K_b(\varepsilon_b - \varepsilon_f)} \quad (1)$$

where [DNA] represents the concentration of ctDNA, ε_a is the apparent extinction coefficient of the complex bound to DNA (A_{obs}/[complex]), ε_f is the extinction coefficient of the free complex, and ε_b is the extinction coefficient of the complex when fully bound to DNA.

The K_b values (Table 1) were identified to be in the range of (1.43–1.79) × 10^4 M^{-1} for ctDNA and (1.79–1.87) × 10^4 M^{-1} for tRNA, in the following order: (**2**) > (**1**) > (**3**). A similar DNA binding behavior has been previously reported for oxovanadium complexes.[45] The binding affinity of the free ligands was significantly lower by approximately one order of magnitude (4.8× 10^3 M^{-1}, and 8.9 × 10^3 M^{-1} for ctDNA and tRNA, respectively) compared to their corresponding vanadium complexes (Table 1).

4.1.2 Emission studies. To further confirm the binding interaction mode between the oxovanadium complexes with ctDNA or tRNA, an ethidium bromide (EB) competitive binding assay was conducted, as the synthesized compounds are non-emissive. Ethidium bromide binds to DNA through intercalation mode, forming a stable EB–DNA adduct with a binding constant which are reported to be in between 10^6 to 10^7 M^{-1}.[48,49] Ethidium bromide (EB) itself exhibits minimal fluorescence; however, it exhibits enhanced fluorescence upon intercalation into the helical structure of DNA. When a competing small molecule is added, a decrease in fluorescence intensity indicates that it displaces EB from EB–DNA/RNA adduct, proposing that the molecule also binds through an intercalative mode.

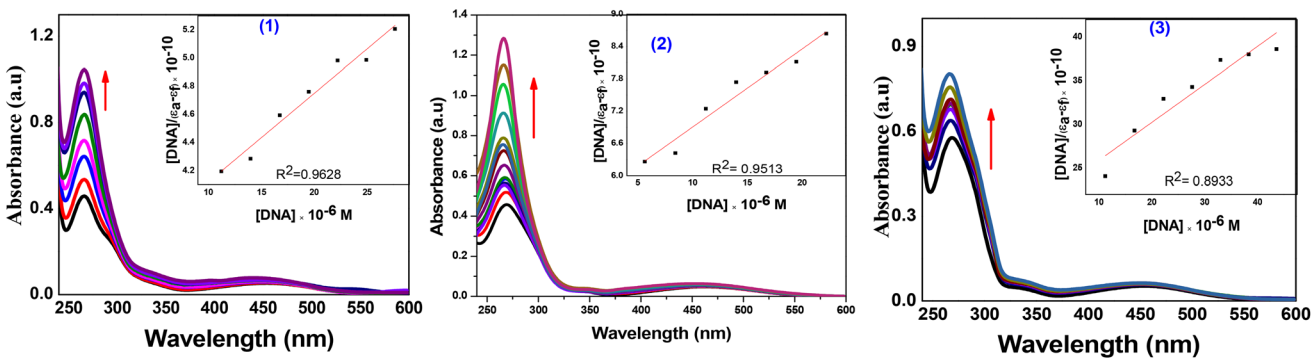

Fig. 3 Changes in the electronic spectra of complexes **1–3** (50 μM) upon titration with ctDNA (0–100 μM) in Tris–HCl buffer (pH 7.2); inset: plot of [DNA] *vs.* [DNA]/(ε_a–ε_f)).

Table 1 Binding constants data (K_b, K_{sv} and K_q) and % hyperchromism of HLw and its vanadium complexes (**1–3**) with ctDNA and tRNA by absorption and emission spectroscopy

	K_b (M^{-1}) × 10^4		% Hyperchromism		(K_{sv}) × 10^4		K_q (M^{-1} S^{-1}) × 10^{10}	
Compd	ctDNA	tRNA	ctDNA	tRNA	ctDNA	tRNA	ctDNA	tRNA
HLw	0.48	0.89	24.4	13.3	0.81	0.70	1.80	1.54
(**1**)	1.76	1.87	55.7	44.8	1.63	2.60	3.58	5.72
(**2**)	2.45	5.1	60	48.0	2.02	3.40	4.44	7.48
(**3**)	1.43	1.79	31.4	22.9	1.06	1.69	2.33	2.70

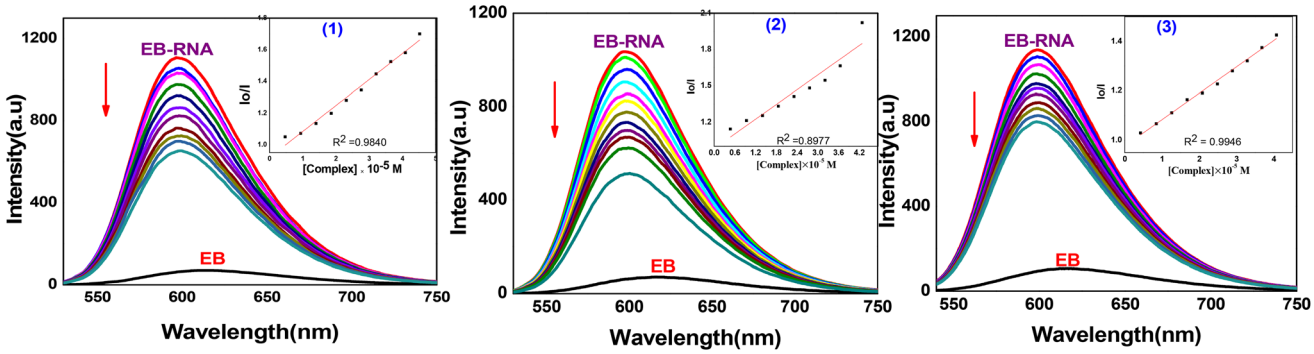

Fig. 4 Effect of complexes **1–3** (0–100 μM) on the fluorescence of the EB–tRNA complex. Inset: Stern–Volmer plots of I_0/I against [complex].

The binding affinity of **1–3** complexes with ctDNA/tRNA was monitored by fluorescence spectroscopy in the wavelength range between (550–750 nm) in PBS (pH 7.2). Both groove binders and intercalators are known to reduce the emission intensity of EB-DNA complexes by either replacing EB or quenching its excited-state electrons *via* a photo-induced electron transfer mechanism.[50] Upon addition of complexes (**1–3**) to the EB–DNA adduct, the fluorescence intensity decreased significantly by approximately hypochromism of 21.8–36.9% for ctDNA and 29.7–50.5% for tRNA. These results revealed that all three oxovanadium complexes competitively interact with ctDNA and tRNA, potentially through an intercalative mode of binding as shown in Fig. S6 and 4, respectively. The Stern–Volmer quenching constant (K_{sv}) was used to evaluate the fluorescence quenching efficiency of the complexes, as calculated from eqn (2) below.[51,52]

$$I_0/I = 1 + K_{sv}[Q] \quad (2)$$

where I_0 and I represent the fluorescence intensities of the complex in the absence and presence of ctDNA or tRNA, respectively. A plot of I_0/I against [complex] yielded a straight line, with the slope corresponding to the K_{sv} values, as shown in Table 1. The quenching constants followed the order (**2**) < (**1**) < (**3**), which aligns with the UV-Vis spectroscopic results.

Furthermore, the bimolecular quenching rate constants (K_q) (Table 1), were calculated using relationship: $K_q = K_{sv}/\tau_o$, (τ_o is a fluorophore's lifetime with values of 22 ns).[53] The calculated values (1.80–4.44 × 10^{10} M^{-1} for ctDNA and 1.54–7.48 × 10^{10} M^{-1} for tRNA are in the order of magnitude higher than (2× 10^{10} M^{-1} S^{-1}, the maximum controlled collision constant). These values support a static quenching mechanism rather than dynamic collision, *i.e.*, indicating formation of a non-fluorescent complex between the compound and ctDNA/tRNA in the ground state. between the metal complexes and the biomolecules in the ground state.[54] Based on the calculated quenching constants, complex 2 shows higher fluorescence quenching efficiency than complexes **1** and **3**, in agreement with the electronic absorption titration data. The quenching and binding constant values suggest that all the **1–3** interact with ctDNA through an intercalation mode.[55]

The interaction with tRNA exhibited a similar behavior to that observed with DNA; however, the binding constants (K_b) were notably higher for tRNA (Table 1), indicating stronger binding affinity compared to DNA.[56] This may be attributed to the distinct structural features of tRNA. Unlike the regular double-helical structure of DNA, tRNA possesses a compact, folded tertiary structure with exposed loops and grooves, offering more accessible and diverse binding sites.[57] Additionally, the higher density of negatively charged phosphate groups on the tRNA surface facilitates stronger electrostatic interactions with the positively charged vanadium (IV/V) complexes. The greater conformational flexibility of tRNA, along with the presence of unique binding pockets in its non-helical regions, may further promote favorable interactions. These factors contribute to the observed increase in binding affinity toward tRNA compared to DNA.[58]

The magnitude of the K_b and K_{sv} values (10^4 M^{-1}) suggests a moderately strong binding affinity toward ctDNA and tRNA base pairs. These values are lower than those reported for the classical intercalator ethidium bromide[48,49,59] which is known for its strong intercalative binding mode. Nevertheless, the obtained binding constants are comparable to, and in some cases better than, those reported for previously studied metal complexes: Cobalt(II) complexes naphthoquinone-based ligand (10^4 M^{-1}),[60] Copper(II) complexes mannich base derived lawsone (10^3 M^{-1}),[61] vanadium(IV) juglone complexes (10^5 M^{-1}),[62] Co(II), Cu(II), Ni(II) and Zn(II) aminonaphthoquinone-based ligand (10^4–10^5 M^{-1},[63] indicating an effective interaction with DNA. Although certain reported systems exhibit higher K_b and K_{sv} values, the binding constants of the present complexes fall within the typical range for metal-based ctDNA binders, supporting their reasonable DNA binding capability.

4.2 Interaction with BSA

The binding of vanadium complexes **1–3** to BSA was studied using UV-Vis and fluorescence spectroscopy to determine the underlying quenching mechanism. Upon the gradual addition (0–100 μM) of the complexes to BSA (50 μM), an increase in the absorption band at 280 nm was observed without any shift in wavelength (Fig. 5), indicating a static quenching mechanism resulting from complex formation in the ground state.[64]

4.2.1 Absorption studies. This method is used to evaluate the disorder within protein structures throughout the interaction with small molecules. The absorption spectra of BSA

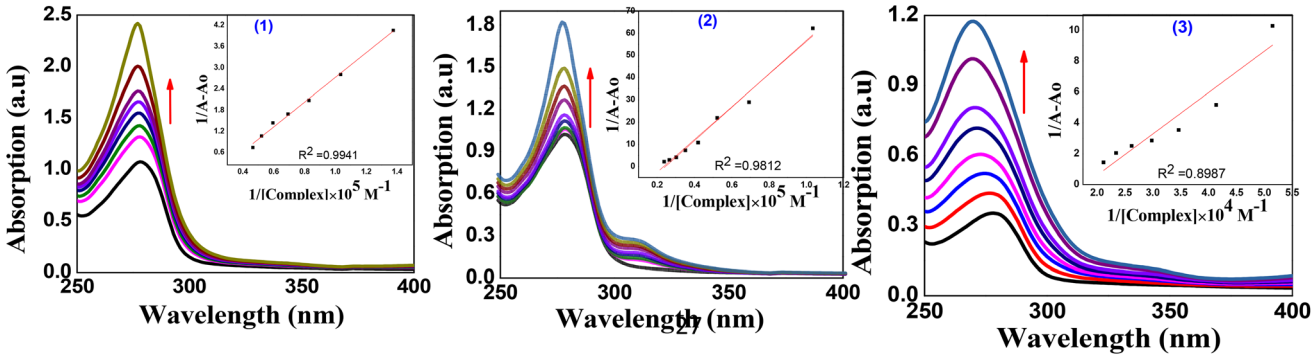

Fig. 5 UV-Vis spectra of BSA (50 μM) with increasing concentrations of complexes **1–3** (0–100 μM) in Tris–HCl buffer (pH 7.2) at 25 °C. Inset: plot of $1/(A - A_0)$ against 1/[complex].

exhibits two distinct bands at roughly 220 and 280 nm, which are assigned to the protein backbone and the phenyl rings of aromatic amino acids; Phe, Trp, and Tyr residues, respectively.[65] The interaction between BSA (50 μM) and vanadium complexes **1–3** was investigated by adding varying concentrations of the complexes (0–100 μM) in Tris–HCl buffer (pH 7.2), with measurements recorded over the wavelength range of 200–350 nm (Fig. 5). An increase in absorbance at 280 nm was observed, along with a hyperchromic effect ranging from 44–70%, with slight blue shift by 1–9 nm suggesting the formation of a new BSA–vanadium complex, which causes an alternation in the microenvironment of the protein residues, and this interaction occurs in the ground state suggesting a static mechanism. The binding parameters between the vanadium complexes and BSA were derived using the eqn (3).[66]

$$1/(A_o - A) = 1/A_o + 1/(K \times A_o \times C_Q) \quad (3)$$

where A_o is the absorbance of free BSA, and A is for BSA after addition of various concentrations of the complexes, respectively, C_Q is the concentration of the test compounds, K is the binding constant obtained from the plot of $1/(A_o - A)$ *vs.* $1/[C_Q]$ from the intercept to the slope ratio. The binding constant of complexes in order of **2**< **1**< **3** and this result agreed with the results of ctDNA and tRNA.

4.2.2 BSA emission studies. To examine conformational changes in BSA induced by complexes **1–3**, fluorescence spectra were recorded using an excitation wavelength of 280 nm, with emission measured from 290 to 450 nm. The intrinsic fluorescence of BSA arises primarily from its aromatic residues; tryptophan, tyrosine, and phenylalanine with the two tryptophan residues being particularly sensitive to the surrounding microenvironment: one is exposed on the protein surface, while the other is buried within the hydrophobic core.[67] 50 μM solution of BSA was titrated with increasing concentrations of vanadium complexes (0–100 μM) in Tris–HCl buffer (pH 7.2). With the addition of the complexes (**1–3**), the emission intensity around 340–350 nm gradually decreased, accompanied by a slight blue shift, indicating conformational changes in BSA and hydrophobic interactions with the complexes as shown in Fig. 6.

The quenching mechanism was further analyzed by the Stern–Volmer eqn (2). A linear relationship between I_o/I and [complex] was observed, from which the Stern–Volmer binding constants (K_{sv}) were determined (Table 2). Among the complexes studied, complex (**2**) exhibited the highest K_{sv} value, consistent with previous results. The bimolecular quenching constants (K_q) were also determined, using τ_0 as 10^{-8} s, confirming a static quenching mechanism.[68]

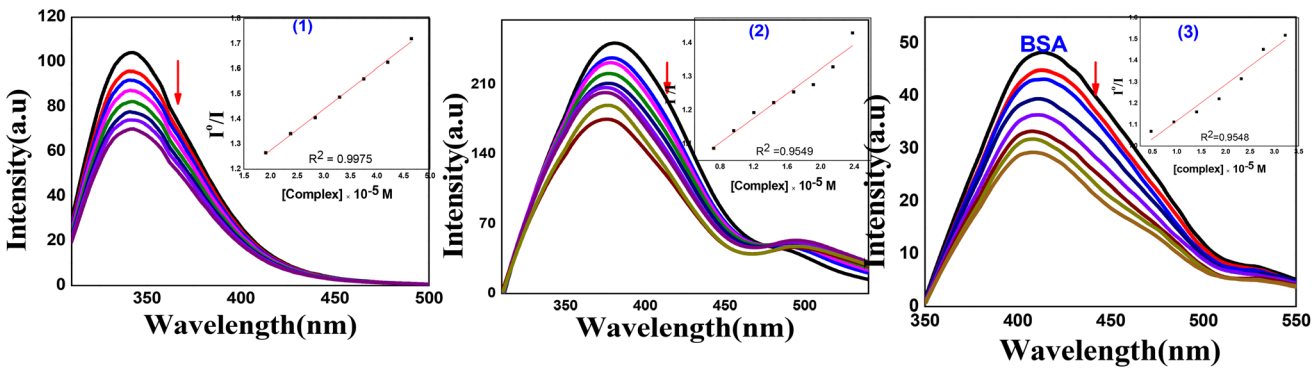

Fig. 6 Fluorescence emission spectra of BSA (50 μM) with increasing concentrations of complexes **1–3** (0–100 μM) in DMSO/PBS. Inset: Stern–Volmer plots showing I_0/I *versus* [complex].

Table 2 The BSA quenching parameters (K_{sv}, K_q, K_b, n, and K_a) of HLw and its complexes (**1–3**)

	Absorption		Emission		
Compd	K_b (M^{-1}) × 10^4	% H[a]	(K_{sv}) ×10^4	K_q (M^{-1} S^{-1}) × 10^{10}	% H[b]
HLw	2.21	−55.3	1.62	1.62	32.9
(**1**)	2.36	−44.0	1.80	1.80	30.4
(**2**)	1.77	−70.0	1.69	1.69	39.6
(**3**)	2.21	−55.3	1.62	1.62	32.9

[a] H, hyperchromism. [b] H hypochromism.

Interestingly, the obtained binding parameters (K_b, K_{sv}, and K_q) indicate that the coordination of lawsone to the metal center does not significantly enhance its binding affinity toward BSA compared to the free ligand. This observation suggests that albumin-mediated transport may not be markedly improved upon complexation, which could be considered a potential limitation.

However, albumin binding represents only one aspect of pharmacokinetic behavior. Metal complexation can impart several important properties, including modulation of lipophilicity, enhanced stability against metabolic degradation, and altered membrane permeability. In addition, metal ions in aqueous solution typically exist as positively charged species capable of interacting with negatively charged biological targets, and they can form coordination complexes with diverse three-dimensional geometries that enable specific molecular recognition. Furthermore, the thermodynamic and kinetic features of metal–ligand interactions, as well as their redox activity and Lewis acidity, contribute significantly to their biological functions and reactivity.[69,70]

In this context, the observed differences between the free ligand and its metal complexes in DNA/RNA binding and cytotoxicity assays support the role of metal coordination in modulating biological activity, even in the absence of enhanced albumin binding.

4.3 Anticancer activity

The cytotoxicity of the newly synthesized V(IV/V) complexes **1–3** and lawsone was assessed using the MTT assay after 24 and 48 hours of treatment in three human cancer cell lines: HeLa (cervical carcinoma), HepG2 (hepatocellular carcinoma), and MCF-7 (breast adenocarcinoma), as well as in normal human lung fibroblasts (WI38). Cisplatin was used as a reference compound for comparison. As summarized in Table 3, the tested complexes exhibited distinct dose- and time-dependent cytotoxic profiles. The calculated IC_{50} values represent the concentration required to reduce cell viability by 50% relative to untreated control cells. Among the compounds investigated, complex **2** demonstrated the highest antiproliferative activity, with an IC_{50} value measured at both 24 and 48 hours in HepG2 cells. This was followed by complex **1** and complex **3**. A similar trend in activity was observed across the tested cancer cell lines, HeLa and MCF7, following the order: complex **2** > complex **1** > complex **3**, as summarized in Table 3. Notably, complex **2** exhibited significantly enhanced cytotoxic activity against HeLa and HepG2 cells at both incubation periods compared to complexes **1**, **3**, and the free ligand. Additionally, complex **2** showed superior activity relative to cisplatin in HeLa cells. However, there was no significant difference in the efficacy of complex **2** compared to cisplatin against HepG2 cells at either time point ($p = 0.926$ and 0.644, respectively). In contrast, the anticancer activity of cisplatin remained superior to that of complex **2** in MCF7 cells for both incubation periods. Furthermore, the free ligand remains superior in its anticancer activity against MCF7 cells compared to our synthesized vanadium complexes, which may indicate that these complexes do not act against breast cancer but are sensitive to other types of cancer. These results highlight the pronounced sensitivity of HepG2 cells to the synthesized vanadium complexes, particularly complex **2**, after 24 hours of incubation. Moreover, a key observation relates to the cytotoxic characteristics of complex **3** in comparison to the lawsone ligand. Although both demonstrated similar IC_{50} values against normal WI38 cells, complex **3** consistently showed higher IC_{50} values across all three cancer cell lines at both 24 and 48 hours, suggesting lower cytotoxic effectiveness against tumor cells compared to the lawsone ligand. This implies that the coordination of vanadium in

Table 3 IC_{50} values of the complexes (**1**), (**2**), and (**3**), and HLw ligand against HeLa, HePG-2, and MCF7 human cancer cell lines and WI38 as normal cell line compared to cisplatin

	Cell lines and selective indices (SI)			
Compd	WI38	Hela	HePG-2	MCF7
24 h				
HLw	51.69 ± 2.9^{a}	39.82 ± 2.3^{b}	47.20 ± 2.6^{b}	9.40 ± 0.7
(**1**)	53.60 ± 3.2^{b}	28.75 ± 1.7^{a}	$30.53 \pm 1.8^{a,b}$	$36.71 \pm 2.1^{a,b}$
(**2**)	$45.77 \pm 2.5^{a,b}$	$15.87 \pm 1.2^{a,b}$	13.73 ± 0.9^{a}	$19.90 \pm 1.3^{a,b}$
(**3**)	$87.26 \pm 4.5^{a,b}$	$51.55 \pm 2.9^{a,b}$	$64.97 \pm 3.7^{a,b}$	$52.95 \pm 3.2^{a,b}$
Cisplatin	25.56 ± 3.2^{a}	24.4 ± 1.63^{a}	12.17 ± 2.1^{a}	5.78 ± 0.48
48 h				
HLw	76.33 ± 4.0^{b}	33.60 ± 2.0^{b}	41.09 ± 2.2^{b}	7.75 ± 0.5
(**1**)	$49.45 \pm 2.7^{a,b}$	$17.86 \pm 1.5^{a,b}$	$23.12 \pm 1.4^{a,b}$	$29.92 \pm 1.9^{a,b}$
(**2**)	$46.34 \pm 2.6^{a,b}$	9.47 ± 0.7^{a}	12.98 ± 0.9^{a}	$11.95 \pm 0.8^{a,b}$
(**3**)	78.53 ± 4.1^{b}	$48.79 \pm 2.8^{a,b}$	$58.77 \pm 3.3^{a,b}$	$42.39 \pm 2.4^{a,b}$
Cisplatin	23.28 ± 1.6^{a}	12.3 ± 1.3^{a}	10.66 ± 1.5^{a}	4.38 ± 0.3

[a] Considered significant compared to ligand ($p \leq 0.05$). [b] Considered significant compared to cisplatin ($p \leq 0.05$).

complex **3** did not result in improved anticancer efficacy and that the inherent cytotoxicity of the lawsone scaffold toward cancer cells was diminished rather than enhanced upon complexation. This behavior can be explained by the presence of 2,2-bipyridine as a co-ligand, which, due to its strong π-acceptor qualities, stabilizes the vanadium center, decreases its electrophilicity, and limits the lability needed for effective interaction with intracellular biomolecular targets such as DNA. Consequently, while the lawsone moiety maintains its natural bioactivity in its uncomplexed form, its cytotoxic ability against cancer cells is lessened within the coordinating environment created by the bpy-vanadium framework. This finding highlights an important structure–activity relationship: the type of additional ligands in vanadium complexes is crucial in determining their biological effectiveness, and although the stabilizing effect of bpy is structurally beneficial, it comes with the drawback of reduced anticancer activity.

Importantly, a differential cytotoxic profile was observed between malignant and non-malignant cells. In the normal WI38 cell line, the vanadium complexes exhibited markedly higher IC_{50} values than in cancer cells, indicating reduced toxicity toward normal cells. It should be mentioned that cisplatin exhibited reduced IC_{50} values against the cancer cell lines that were tested, when compared to the complexes being studied, which underscores its recognized effectiveness as a clinically refined platinum-based drug that operates through a direct DNA platination mechanism. In contrast, cisplatin retained substantial cytotoxicity in WI38 cells, reflecting its well-known non-selective behavior due to its DNA-targeting in both normal and cancer cells.[71] Overall, these findings underscore the superior and selective anticancer potential of complex **2**, which is comparable to or, in certain cases, exceeds that of cisplatin. This selective cytotoxicity is further supported by the calculated selectivity index (SI) values, underscoring their potential as safer anticancer candidates.

To demonstrate the safety of the complexes on normal cells, we assess the SIs. The cytotoxicity ratios of complexes (**1**, **2**, and **3**), the ligand, and cisplatin against WI38 cells were compared to those of HePG2, MCF7, and HeLa cell lines to calculate the selectivity index. The higher the SI values of a compound, the higher the anticancer activity and safety.[72] The SIs of the compounds with SI values larger than 3 are regarded as very selective.[73] Complex **2** exhibited the highest anticancer activity among the tested vanadium complexes (**1–3**), the free ligand, and cisplatin in both HeLa and HepG2 cells. Notably, complex **2** demonstrated excellent selectivity across all tested cancer cell lines, with SIs ranging from 2.88 to 4.89 in HeLa, 3.33 to 3.57 in HepG2, and 2.30 to 3.87 in MCF7 cells at 24 and 48 hours, all surpassing the SIs of cisplatin. These results highlight the compound's potent anticancer potential combined with a favorable safety profile toward normal WI38 cells. In contrast, the free ligand showed lower selectivity in HeLa and HepG2 cells but surprisingly exhibited the highest SI values in MCF7 cells (5.49 at 24 h and 9.84 at 48 h), exceeding both the vanadium complexes and cisplatin. Complex **1** also demonstrated improved selectivity over cisplatin in HeLa and MCF7 cells, with a 1.46-fold increase in SI in HeLa and a 5.15-fold increase in MCF7 at 48 h. These findings indicate that while coordination with vanadium generally enhances anticancer activity, it may also increase toxicity toward normal cells, slightly narrowing the therapeutic window in certain contexts, such as in MCF7 cells. Another mentioned observation, complexes **1** and **2** exhibited significantly higher SI values in comparison to cisplatin across various cell lines and time intervals, suggesting a substantially broader therapeutic range, even though their absolute IC_{50} values are higher. These results emphasize a critical limitation of the current compounds, which is their reduced cytotoxic effectiveness relative to the reference drug, and highlight the necessity for additional structural refinement to enhance both activity and selectivity at the same time.

Finally, it is recognized that the current evaluation of cytotoxicity was performed at 24 and 48 h of incubation, which are standard time intervals commonly used in studies of vanadium metal complex cytotoxicity.[74–76] The potential for extended incubation at 72 h to show different activity profiles, especially for complex **3** and HLw, cannot be omitted. Future research directions should include extended time-point studies, as well as mechanistic investigations and *in vivo* validation of the identified anticancer activity, in order to thoroughly determine the biological profile of these complexes.

Structure–activity relationships (SAR) of the vanadium complexes reveal that their reactivity is strongly influenced by both the ligand structure and the oxidation state, which in turn dictate their biological behavior. In the extracellular environment, vanadium exists mainly as pentavalent vanadate V(v). In contrast, inside cells, it is predominantly present as tetravalent vanadyl V(IV) species. This indicates that vanadium-based complexes may become activated by reduction within the cellular environment, which is considered an important step for their biological activity.[2,75,77,78] The redox characteristics of vanadium are influenced by its specific electronic configurations in different oxidation states. V(v), possessing a d^0 configuration and a relatively high positive charge, can engage in strong electrostatic interactions with the negatively charged phosphate backbone of DNA and RNA. In contrast, V(IV), with a d^1 configuration, exhibits greater kinetic lability. For biologically active metal complexes, a certain degree of metal–ligand lability is often required to allow ligand exchange and interaction with intracellular biomolecular targets, hence we correlate the higher activity of V(v) over V(IV) complexes.[79,80] However, for complex **3**, the incorporation of 2,2′-bipyridine as a co-ligand leads to a marked decrease in DNA-binding ability, which is consistent with the experimentally observed lower biological activity. Bipyridine acts as a π-acceptor ligand, stabilizing the metal center and decreasing its electrophilicity, thereby weakening its interaction with nucleophilic biomolecular targets such as DNA. Consequently, complexes containing bpy ligands generally exhibit reduced DNA/RNA binding affinity and diminished biological activity. The strong chelation, rigid planar geometry, and decreased lability of bpy result in limited interaction with biomolecular targets, consistent with similar observations in the literature.[81]

4.4 SOD-like activity

The SOD-like activity assay relies on the capacity of the tested complexes to transfer electrons or $O_2^{\bullet -}$ to NBT, and hence inhibiting it, which leads to the transformation of the yellow tetrazolium into a blue precipitate.[82] Our results demonstrated that complex **2** exhibited the highest SOD-like activity, followed by complex **1** and then complex **3**, with IC_{50} values of 10.267 ± 0.536, 12.567 ± 0.636, and 21.630 ± 2.340, respectively. This indicates that complex **2** has the greatest capability for superoxide scavenging, revealing its strong antioxidant activity (Fig. 7A).

4.5 α-Amylase inhibition

Albumin, the predominant protein in blood plasma, is essential for transporting drugs and distributing them across different tissues. The capacity of vanadium complexes to bind to BSA is therefore particularly relevant, as it can influence their bioavailability and systemic stability. In the context of diabetes, hyperglycemia arises from impaired glucose homeostasis, where salivary and pancreatic α-amylases initiate carbohydrate metabolism.[73,83,84] The antidiabetic activity of the three vanadium complexes (**1–3**) (Fig. 7B) and the free ligand was evaluated based on their ability to inhibit α-amylase, with IC_{50} values determined for each. The inhibitory effect of all compounds increased with concentration, consistent with their albumin-binding capacity. Among the tested compounds, complex **2** exhibited the highest α-amylase inhibition (IC_{50} = 0.35 ± 0.042 μM), followed by complex **3** (IC_{50} = 0.443 ± 0.029 μM), the free ligand (IC_{50} = 0.946 ± 0.041 μM), and complex **1** (IC_{50} = 1.017 ± 0.016 μM), whereas the standard antidiabetic drug acarbose showed an IC_{50} of 0.160 ± 0.029 μM. This dual action-enzyme inhibition and efficient albumin-mediated delivery-likely underlies the observed antidiabetic effects, as the high BSA-binding affinity of complex 2 may prevent α-amylase from breaking down starch into glucose, highlighting it as a promising candidate for further investigation due to its potent inhibitory activity and favorable transport properties.

4.6 Antibacterial activity

The complexes (10 μg per disc) were tested against two Gram-positive and two Gram-negative bacterial strains. All complexes exhibited good antibacterial activity, with inhibition

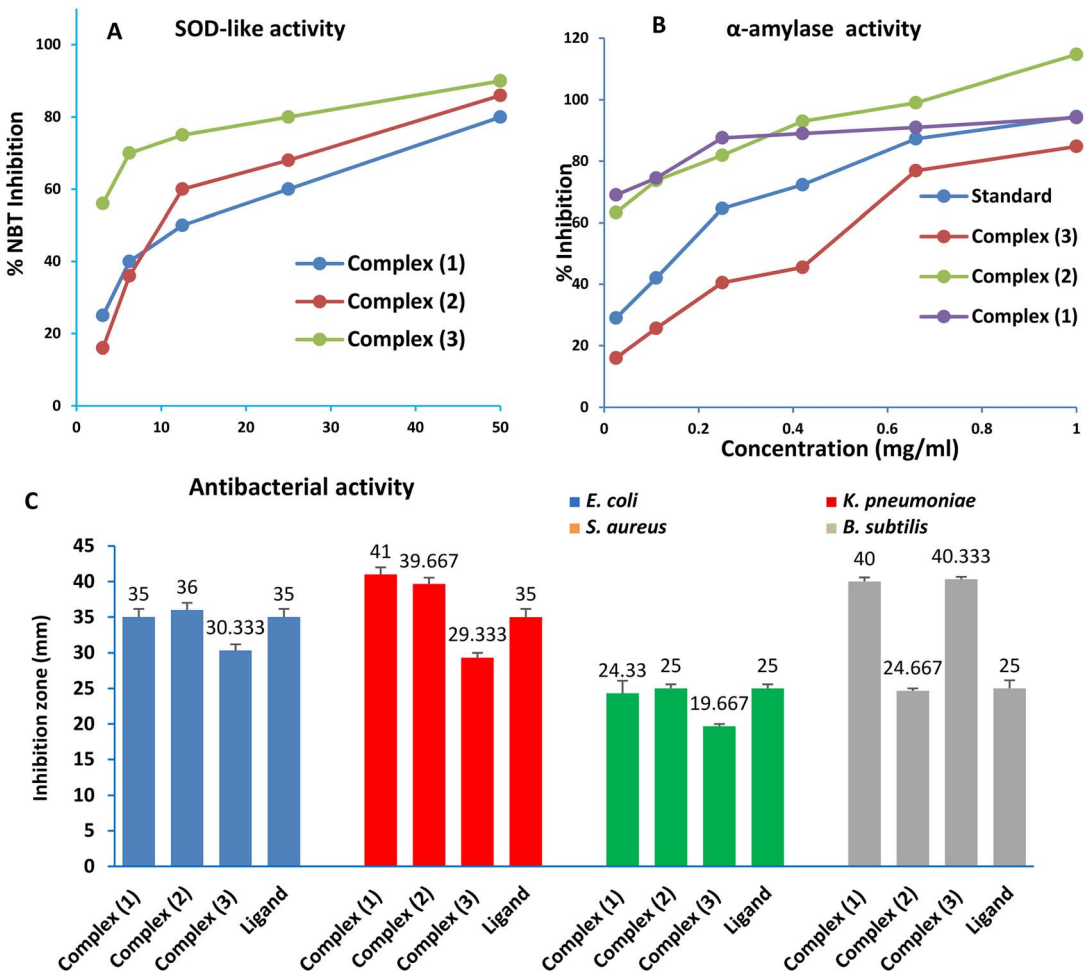

Fig. 7 Percentage of NBT inhibition with increasing the concentration of the three vanadium complexes (A). The *in vitro* antidiabetic activity of the three vanadium complexes and acarbose by α-amylase enzyme inhibition assay (B). Bar plots represent the antibacterial activities of the three vanadium complexes and ligand (C).

zones exceeding 10 mm (Fig. 7C). Complexes (**1**) and (**2**) demonstrated greater effectiveness against *E. coli*, *K. pneumoniae*, and *S. aureus* compared to complex (**3**). In contrast, complexes (**1**) and (**3**) exhibited higher activity against *B. subtilis* than complex (**2**). For the ligand, antibacterial activity was lower against the two Gram-negative strains (*E. coli* and *K. pneumoniae*) compared to complexes (**1**) and (**2**). However, against *B. subtilis*, the ligand showed reduced antibacterial activity compared to complexes (**1**) and (**3**) but had equal activity to complex (**2**) (Fig. 7C). These findings indicate that different vanadium complexes exhibit varying levels of antibacterial activity and that the choice of suitable organic ligands coordinated with the vanadium component significantly affects the antibacterial effectiveness of each complex. Several studies support our results, showing that the coordination of vanadium with ligands enhances the antibacterial activity of the synthesized complexes.[82,85–87]

4.7 Molecular docking

The molecular docking simulations of LW with BSA and for Complex **2** with both BSA and α-amylase (Fig. 8) provide valuable structural insight into its potential transport behavior and enzymatic inhibition profile. These simulations were conducted exclusively for complex 2 due to its superior biological activity observed experimentally, making it the most relevant candidate for detailed structure–activity relationship analysis. In addition, the three investigated complexes share a high degree of structural similarity, including the same metal center and closely related ligand frameworks, differing only in minor substituent features. Therefore, their binding modes and interaction profiles are expected to be largely comparable. Under this assumption, detailed docking analysis of complex 2 can provide representative atomistic insights that are broadly applicable to the entire series.

Initially, docking of LW to BSA has been conducted and the results indicate that LW binds favorably within the BSA binding pocket with a calculated binding energy of −5.82 kcal mol^{-1}, suggesting a moderate and stable interaction. From the docking pose, the ligand is positioned along the α-helical region and is stabilized primarily through non-covalent interactions. Key residues involved include Gln579, Phe509, and His534.

The optimized docking poses for complex (2) with both BSA and α-amylase reveal stable binding conformations within well-defined pockets of both proteins, supported by a network of electrostatic and hydrogen-bonding interactions. In the case of BSA, Complex **2** is deeply embedded within a hydrophobic cavity of the protein with a favorable binding energy of −9.09 kcal mol^{-1}, higher and thus more potent than the binding of the LW alone. The binding environment for the bound complex (2) is dominated by positively charged residues, particularly Arg144, Lys144, and Arg185, which are located in close proximity to the vanadium coordination sphere. The negatively polarized regions of the complex—mainly localized over the oxo and phenolate oxygen atoms—favor strong electrostatic interactions with these basic residues. In addition, hydrogen bonding interactions may occur between the coordinated oxo group and the guanidinium side chains of arginine residues. The aromatic framework of the hydroxynaphthoquinone ligands is oriented toward hydrophobic regions of the cavity, enabling π–π and van der Waals interactions that further stabilize the complex–protein adduct. The combined electrostatic complementarity and hydrophobic contacts suggest an efficient albumin-binding capability, which is essential for metal-based drugs as albumin acts as a carrier protein in the bloodstream. Such binding may enhance the stability, solubility, and systemic transport of the complex under physiological conditions. Importantly, the binding of LW into BSA, is distinct from that observed for the vanadium–containing complex 2, where metal coordination and additional electrostatic contributions play a more significant role. In contrast, the LW ligand relies primarily on classical non-covalent interactions, leading to a different binding orientation and weaker interaction profile within BSA. This later observation clearly underline the role of vanadium coordination in enhancing the binding affinity and thus the biological activity.

For α-amylase, Complex **2** adopts a well-oriented conformation near the enzyme's active-site region with a docking score of −6.75 kcal mol^{-1}. The docking pose indicates close contacts with residues such as Gln163 and Asn105, which are capable of forming hydrogen bonds through their amide side chains. The oxo group and phenolic oxygen atoms of the complex act as hydrogen-bond acceptors, promoting stabilizing interactions with these polar residues. Furthermore, the planar aromatic ligands are positioned to interact with nearby hydrophobic or π-rich residues, reinforcing the binding through dispersive and

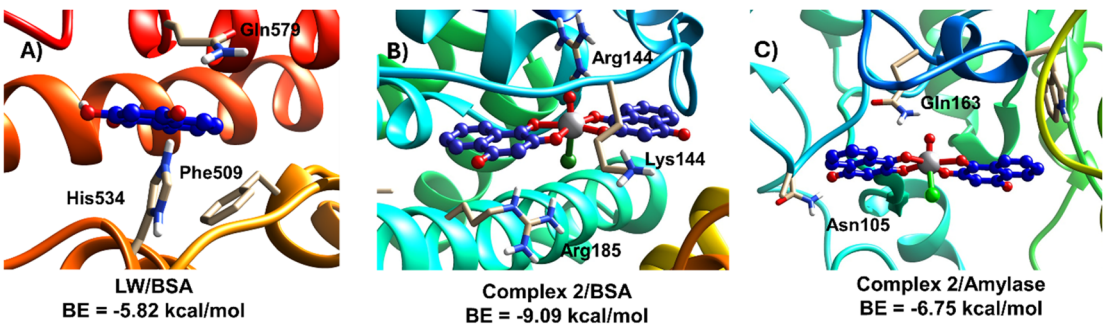

Fig. 8 The obtained docked complexes for (A) LW-ligand with BSA, (B) Complex (**2**)/BSA and (C) Complex (**2**)/α-amylase.

stacking interactions. The orientation of the complex within the catalytic pocket suggests potential interference with substrate access or catalytic residues, indicating a plausible inhibitory effect on α-amylase activity.

Overall, the docking results demonstrate that Complex **2** exhibits favorable binding toward both serum albumin and α-amylase through a combination of electrostatic attraction, hydrogen bonding, and hydrophobic/π-interactions. The strong interaction with albumin supports effective biological transport, while its stable accommodation within the α-amylase active site suggests potential enzymatic inhibition. These findings collectively highlight the dual role of Complex **2** in protein binding and enzyme targeting, which may contribute to its observed biological activity.

5 Conclusions

In this work, three oxovanadium(IV/V) complexes (**1–3**) based on lawsone were synthesized and characterized, confirming the monoanionic bidentate O, O-coordination mode and the formation of stable coordination compounds. The biological studies demonstrated that all complexes exhibit moderate binding affinity toward ctDNA, tRNA, and BSA, with binding constants in the order of 10^4 M^{-1}, indicating their ability to interact with key biomacromolecules. Among the series, complex $[VO(Lw)_2Cl]$ (**2**) showed consistently superior performance, exhibiting the strongest biomolecular interactions, which correlated well with its enhanced *in vitro* cytotoxic activity against HeLa, HepG2, and MCF-7, along with higher selectivity compared to cisplatin and reduced toxicity toward WI-38 cells. The improved therapeutic profile of complex (**2**) can be attributed to its favorable redox properties, which collectively promote effective interactions with nucleic acids and proteins. In addition, the complexes showed measurable antioxidant activity with SOD-like $IC_{50} = 10.27 \pm 0.54$ μM, along with moderate antibacterial effects against both Gram-positive and Gram-negative bacterial strains and significant α-amylase inhibition ($IC_{50} = 0.35 \pm 0.04$ μM), suggesting the presence of complementary bioactivities beyond anticancer potential. DFT calculations and molecular docking studies further supported the experimental findings by revealing favorable electronic distribution and stable interactions with biological receptors through hydrogen bonding, electrostatic, and π-interactions. Overall, the results highlight that the biological activity of vanadium-lawsone complexes is greatly influenced by the metal oxidation state and ligand environment. The combined experimental and computational data provide useful structure–activity relationships insights for the rational design of future vanadium-based metallodrugs.

Author contributions

Islam M. Elnabky methodology, software, formal analysis. Mohamed M. Aboelnga: supervision, software, validation, formal analysis, writing – review & editing. Heba A. Sahyon, resources, software, validation, writing – review & editing. Ahmed M. El-Hendawy: supervision, resources, writing – review & editing. Shadia A. Elsayed: supervision, conceptualization, formal analysis, resources, visualization, validation, writing – review & editing.

Conflicts of interest

The authors declare no conflicts of interest.

Data availability

The data supporting this article have been included as part of the supplementary information (SI). Supplementary information: experimental procedures, spectroscopic characterization (FT-IR, ^{1}H NMR, ESI-MS), thermal analysis (TGA), and additional figures related to nucleic acid (ctDNA/tRNA) and protein (BSA) interaction studies of the synthesized complexes. See DOI: https://doi.org/10.1039/d6ra02275h.

Acknowledgements

The authors thank the Ministry of Higher Education, Egypt, for their support of the CIQAP project (CP3-016-MAN), and the Academy of Scientific Research and Technology (ASRT) for funding research equipment *via* the Science Up Capacity Building initiative (Grant No. 6389).

References

1 L. Marzban, R. Rahimian, R. W. Brownsey and J. H. McNeill, Mechanisms by which Bis(Maltolato)Oxovanadium(IV) Normalizes Phosphoenolpyruvate Carboxykinase and Glucose-6-Phosphatase Expression in Streptozotocin-Diabetic Rats *in Vivo*, *Endocrinology*, 2002, **143**, 4636–4645.
2 J. C. Pessoa, S. Etcheverry and D. Gambino, Vanadium compounds in medicine, *Coord. Chem. Rev.*, 2015, **301–302**, 24–48.
3 A. R. Saltiel and C. R. Kahn, Insulin signalling and the regulation of glucose and lipid metabolism, *Nature*, 2001, **414**, 799–806.
4 S. P. Dash, A. K. Panda, S. Pasayat, S. Majumder, A. Biswas, W. Kaminsky, S. Mukhopadhyay, S. K. Bhutia and R. Dinda, Evaluation of the cell cytotoxicity and DNA/BSA binding and cleavage activity of some dioxidovanadium(V) complexes containing aroylhydrazones, *J. Inorg. Biochem.*, 2015, **144**, 1–12.
5 P. K. Sasmal, A. K. Patra and A. R. Chakravarty, Synthesis, structure, DNA binding and DNA cleavage activity of oxovanadium(IV) N-salicylidene-*S*-methyldithiocarbazate complexes of phenanthroline bases, *J. Inorg. Biochem.*, 2008, **102**, 1463–1472.
6 S. P. Dash, S. Pasayat, H. R. Dash, S. Das, R. J. Butcher and R. Dinda, Oxovanadium (V) complexes incorporating tridentate aroylhydrazoneoximes: synthesis, characterizations and antibacterial activity, *Polyhedron*, 2012, **31**, 524–529.
7 D. Rehder, Import and Implications of Vanadium in Live Aspects, *Inorganics*, 2023, **11**, 256.

8 K. Singh, P. Patel and A. Goswami, Anti-Inflammatory Activity of Hydroxytriazenes and their Vanadium Complexes, *J. Chem.*, 2008, **5**, 1144–1148.
9 A. M. Evangelou, Vanadium in cancer treatment, *Crit. Rev. Oncol. Hematol.*, 2002, **42**, 249–265.
10 I. S. Mahmoud, H. Hyari, E. Esawi and W. Alshaer, Anti-tumour signalling pathways and molecular targets of 1,4-naphthoquinone-based natural dyes, *Nat. Prod. Res.*, 2025, 1–20.
11 M. Saini, V. Kumar, S. Chauhan, V. Sharma and P. K. Dhakad, Exploring Synthetic Strategies and Therapeutic Potential of Naphthoquinone Derivatives: A Review, *J. Heterocycl. Chem.*, 2025, **62**, 1898–1915.
12 C. E. Pereyra, R. F. Dantas, S. B. Ferreira, L. P. Gomes and F. P. Silva-Jr, The diverse mechanisms and anticancer potential of naphthoquinones, *Cancer Cell Int.*, 2019, **19**, 207.
13 N. Mone, S. Harihar, S. Salunke-Gawali, S. Satpute, A. Patil, V. Mokashi, M. Jadhav and R. J. Butcher, Metal complexes of 'Heena' (2-hydroxy-1,4-naphthoquinone): Synthesis, Characterization and anticancer activity, *Inorg. Chim. Acta*, 2023, **546**, 121290.
14 S. P. Devi, S. Kumaria, S. R. Rao and P. Tandon, Carnivorous Plants as a Source of Potent Bioactive Compound: Naphthoquinones, *Trop. Plant Biol.*, 2016, **9**, 267–279.
15 F. S. S. Selvaraj, M. Samuel, A. K. Karuppiah and N. Raman, Transition metal complexes incorporating lawsone: a review, *J. Coord. Chem.*, 2022, **75**, 2509–2532.
16 M. N. Abo Elenen, A. R. Elshobaky and S. A. Elsayed, New Silver(I) Lawsone-based complexes: Synthesis, characterization, interaction with biological macromolecules, *in vitro* antineoplastic, antimetastatic, and antimicrobial activity, *J. Mol. Struct.*, 2024, **1317**, 139048.
17 S. Oramas-Royo, C. Torrejon, I. Cuadrado, R. Hernandez-Molina, S. Hortelano, A. Estevez-Braun and B. de Las Heras, Synthesis and cytotoxic activity of metallic complexes of lawsone, *Bioorg. Med. Chem.*, 2013, **21**, 2471–2477.
18 P. Jeyaraman, M. Samuel, A. Johnson and N. Raman, Synthesis, characterization, ADMET, *in vitro* and *in vivo* studies of mixed ligand metal complexes from a curcumin Schiff base and lawsone, *Nucleosides, Nucleotides Nucleic Acids*, 2020, **40**, 242–263.
19 L. Tabrizi, R. Golbang, H. Sadeghi, H. Chiniforoshan, P. Mcardle and B. Notash, Dinuclear cadmium indomethacin and Lawsone complexes: synthesis, crystal structures, antiproliferative and biological evaluations, *J. Coord. Chem.*, 2016, **69**, 3021–3034.
20 A. P. Neves, M. X. Pereira, E. J. Peterson, R. Kipping, M. D. Vargas, F. P. Silva-Jr, J. W. M. Carneiro and N. P. Farrell, Exploring the DNA binding/cleavage, cellular accumulation and topoisomerase inhibition of 2-hydroxy-3-(aminomethyl)-1, 4-naphthoquinone Mannich bases and their platinum (II) complexes, *J. Inorg. Biochem.*, 2013, **119**, 54–64.
21 M. N. A. Elenen, A. R. Elshobaky and S. A. Elsayed, New Silver (I) Lawsone-based complexes: Synthesis, characterization, interaction with biological macromolecules, *in vitro* antineoplastic, antimetastatic, and antimicrobial activity, *J. Mol. Struct.*, 2024, **1317**, 139048.
22 P. Nariya, S. Prajapati and S. Thakore, Vanadium (IV) Complex Synthesized Using Natural Product Lawsone as Efficient Catalyst for Oxidation of Activated sp^3 C−H Bond, *ChemistrySelect*, 2023, **8**, e202302819.
23 S. Samanta, D. Ghosh, S. Mukhopadhyay, A. Endo, T. J. Weakley and M. Chaudhury, Oxovanadium (IV) and-(V) complexes of dithiocarbazate-based tridentate schiff base ligands: syntheses, structure, and photochemical reactivity of compounds involving imidazole derivatives as coligands, *Inorg. Chem.*, 2003, **42**, 1508–1517.
24 F. Denizot and R. Lang, Rapid colorimetric assay for cell growth and survival: modifications to the tetrazolium dye procedure giving improved sensitivity and reliability, *J. Immunol. Methods*, 1986, **89**, 271–277.
25 N.-C. Yang, C.-C. Wu, R. H. Liu, Y.-C. Chai and C. Y. Tseng, Comparing the functional components, SOD-like activities, antimutagenicity, and nutrient compositions of Phellinus igniarius and Phellinus linteus mushrooms, *J. Food Drug Anal.*, 2016, **24**, 343–349.
26 C. J. Ononamadu, A. J. Alhassan, A. A. Imam, A. Ibrahim, G. O. Ihegboro, A. T. Owolarafe and M. S. Sule, *In vitro* and *in vivo* anti-diabetic and anti-oxidant activities of methanolic leaf extracts of Ocimum canum, *Caspian J. Intern. Med.*, 2019, **10**, 162.
27 C. Valgas, S. M. d. Souza, E. F. Smânia and A. Smânia Jr, Screening methods to determine antibacterial activity of natural products, *Braz. J. Microbiol.*, 2007, **38**, 369–380.
28 D. Halarnekar, M. Ayyanar, P. Gangapriya, M. Kalaskar, V. Redasani, N. Gurav, S. Nadaf, S. Saoji, N. Rarokar and S. Gurav, Eco synthesized chitosan/zinc oxide nanocomposites as the next generation of nano-delivery for antibacterial, antioxidant, antidiabetic potential, and chronic wound repair, *Int. J. Biol. Macromol.*, 2023, **242**, 124764.
29 A. D. Becke, Density-functional thermochemistry. III. The role of exact exchange, *J. Chem. Phys.*, 1993, **98**, 5648–5652.
30 C. Lee, W. Yang and R. G. Parr, Development of the Colle-Salvetti correlation-energy formula into a functional of the electron density, *Phys. Rev. B: Condens. Matter Mater. Phys.*, 1988, **37**, 785.
31 P. J. Stephens, F. J. Devlin, C. F. Chabalowski and M. J. Frisch, Ab initio calculation of vibrational absorption and circular dichroism spectra using density functional force fields, *J. Phys. Chem.*, 1994, **98**, 11623–11627.
32 S. H. Vosko, L. Wilk and M. Nusair, Accurate spin-dependent electron liquid correlation energies for local spin density calculations: a critical analysis, *Can. J. Phys.*, 1980, **58**, 1200–1211.
33 S. Grimme, A. Hansen, J. G. Brandenburg and C. Bannwarth, Dispersion-corrected mean-field electronic structure methods, *Chem. Rev.*, 2016, **116**, 5105–5154.
34 M. M. Aboelnga, H. A. Sahyon and S. A. Elsayed, Synthesis and characterization of novel Ru (III) complexes of 2-aminopyrazine: Interaction with biomolecules,

antineoplastic activity, and computational investigation, *Appl. Organomet. Chem.*, 2024, **38**, e7427.

35 S. A. Elsayed, E. E. Saleh, M. M. Aboelnga and E. A. Toson, Experimental and computational studies of silver(I) dibenzoylmethane-based complexes, interaction with DNA/RNA/BSA biomolecules, and *in vitro* cytotoxic activity, *J. Inorg. Biochem.*, 2023, **241**, 112132.

36 G. M. Morris, R. Huey, W. Lindstrom, M. F. Sanner, R. K. Belew, D. S. Goodsell and A. J. Olson, AutoDock4 and AutoDockTools4: Automated docking with selective receptor flexibility, *J. Comput. Chem.*, 2009, **30**, 2785–2791.

37 L. Goldbach, B. J. A. Vermeulen, S. Caner, M. Liu, C. Tysoe, L. van Gijzel, R. Yoshisada, M. Trellet, H. van Ingen, G. D. Brayer, A. M. J. J. Bonvin and S. A. K. Jongkees, Folding Then Binding *vs.* Folding Through Binding in Macrocyclic Peptide Inhibitors of Human Pancreatic α-Amylase, *ACS Chem. Biol.*, 2019, **14**, 1751–1759.

38 I. M. Elnabky, M. M. Aboelnga, H. M. El-Gharabawy, S. A. Elsayed and A. M. El-Hendawy, Dehydroacetic acid benzoyl hydrazone complexes of Ni(II) and Pd(II): Synthesis, characterization, computational studies, biomolecular interaction, and dual anticancer–antimicrobial activities, *Inorg. Chim. Acta*, 2026, **593**, 123047.

39 E. F. Pettersen, T. D. Goddard, C. C. Huang, G. S. Couch, D. M. Greenblatt, E. C. Meng and T. E. Ferrin, UCSF Chimera—a visualization system for exploratory research and analysis, *J. Comput. Chem.*, 2004, **25**, 1605–1612.

40 S. Samanta, D. Ghosh, S. Mukhopadhyay, A. Endo, T. J. R. Weakley and M. Chaudhury, Oxovanadium(IV) and -(V) Complexes of Dithiocarbazate-Based Tridentate Schiff Base Ligands: Syntheses, Structure, and Photochemical Reactivity of Compounds Involving Imidazole Derivatives as Coligands, *Inorg. Chem.*, 2003, **42**, 1508–1517.

41 E. Kwiatkowski, G. Romanowski, W. Nowicki, M. Kwiatkowski and K. Suwińska, Dioxovanadium(V) Schiff base complexes of N-methyl-1,2-diaminoethane and 2-methyl-1,2-diaminopropane with aromatic o-hydroxyaldehydes and o-hydroxyketones: synthesis, characterisation, catalytic properties and structure, *Polyhedron*, 2003, **22**, 1009–1018.

42 D. I. Tofiq, H. Q. Hassan and K. A. Abdalkarim, Preparation of a novel Mixed-Ligand divalent metal complexes from solvent free Synthesized Schiff base derived from 2,6-Diaminopyridine with cinnamaldehyde and 2,2′-Bipyridine: Characterization and antibacterial activities, *Arab. J. Chem.*, 2021, **14**, 103429.

43 D. Hesek, Y. Inoue, S. R. L. Everitt, H. Ishida, M. Kunieda and M. G. B. Drew, Preparation and structural elucidation of novel cis ruthenium(II) bis(bipyridine) sulfoxide complexes, *J. Chem. Soc., Dalton Trans.*, 1999, 3701–3709.

44 T. Ghosh, S. Bhattacharya, A. Das, G. Mukherjee and M. G. B. Drew, Synthesis, structure and solution chemistry of mixed-ligand oxovanadium(IV) and oxovanadium(V) complexes incorporating tridentate ONO donor hydrazone ligands, *Inorg. Chim. Acta*, 2005, **358**, 989–996.

45 S. A. Aboafia, S. A. Elsayed, A. K. A. El-Sayed and A. M. El-Hendawy, New transition metal complexes of 2,4-dihydroxybenzaldehyde benzoylhydrazone Schiff base (H2dhbh): Synthesis, spectroscopic characterization, DNA binding/cleavage and antioxidant activity, *J. Mol. Struct.*, 2018, **1158**, 39–50.

46 A. A. Holder, P. Taylor, A. R. Magnusen, E. T. Moffett, K. Meyer, Y. Hong, S. E. Ramsdale, M. Gordon, J. Stubbs, L. A. Seymour, D. Acharya, R. T. Weber, P. F. Smith, G. C. Dismukes, P. Ji, L. Menocal, F. Bai, J. L. Williams, D. M. Cropek and W. L. Jarrett, Preliminary anti-cancer photodynamic therapeutic *in vitro* studies with mixed-metal binuclear ruthenium(II)-vanadium(IV) complexes, *Dalton Trans.*, 2013, **42**, 11881–11899.

47 D. Patra, S. Paul, I. Majumder, N. Sepay, S. Bera, R. Kundu, M. G. B. Drew and T. Ghosh, Exploring the effect of substituent in the hydrazone ligand of a family of μ-oxidodivanadium(v) hydrazone complexes on structure, DNA binding and anticancer activity, *Dalton Trans.*, 2017, **46**, 16276–16293.

48 A. Alonso, M. J. Almendral, Y. Curto, J. J. Criado, E. Rodríguez and J. L. Manzano, Determination of the DNA-binding characteristics of ethidium bromide, proflavine, and cisplatin by flow injection analysis: Usefulness in studies on antitumor drugs, *Anal. Biochem.*, 2006, **355**, 157–164.

49 M. J. Waring, Complex formation between ethidium bromide and nucleic acids, *J. Mol. Biol.*, 1965, **13**, 269–282.

50 J. K. Barton, J. M. Goldberg, C. V. Kumar and N. J. Turro, Binding modes and base specificity of tris(phenanthroline) ruthenium(II) enantiomers with nucleic acids: tuning the stereoselectivity, *J. Am. Chem. Soc.*, 1986, **108**, 2081–2088.

51 E. A. Permyakov, *Luminescent Spectroscopy of Proteins*, CRC press, 2018.

52 A. S. Ladokhin, Fluorescence spectroscopy in peptide and protein analysis, *Encycl. Anal. Chem.*, 2000, 5762–5779.

53 K. S. Ghosh, B. K. Sahoo, D. Jana and S. Dasgupta, Studies on the interaction of copper complexes of (−)-epicatechin gallate and (−)-epigallocatechin gallate with calf thymus DNA, *J. Inorg. Biochem.*, 2008, **102**, 1711–1718.

54 M. Anjomshoa, S. J. Fatemi, M. Torkzadeh-Mahani and H. Hadadzadeh, DNA-and BSA-binding studies and anticancer activity against human breast cancer cells (MCF-7) of the zinc (II) complex coordinated by 5, 6-diphenyl-3-(2-pyridyl)-1, 2, 4-triazine, *Spectrochim. Acta, Part A*, 2014, **127**, 511–520.

55 M. Neelakantan, C. Balakrishnan, V. Selvarani and M. Theetharappan, DNA/BSA binding interactions and VHPO mimicking potential of vanadium (IV) complexes: Synthesis, structural characterization and DFT studies, *Appl. Organomet. Chem.*, 2018, **32**, e4125.

56 K. Suntharalingam and R. Vilar, Interaction of metal complexes with nucleic acids, *Annu. Rep. Prog. Chem., Sect. A:Inorg. Chem.*, 2011, **107**, 339–358.

57 J. I. Gyi, G. L. Conn, A. N. Lane and T. Brown, Comparison of the Thermodynamic Stabilities and Solution Conformations of DNA·RNA Hybrids Containing Purine-Rich and Pyrimidine-Rich Strands with DNA and RNA Duplexes, *Biochemistry*, 1996, **35**, 12538–12548.

58 R. T. Wheelhouse and J. B. Chaires, Drug Binding to DNA·RNA Hybrid Structures, in *Drug-DNA Interaction Protocols*, ed. K. R. Fox, Humana Press, Totowa, NJ, 2010, pp. 55–70.
59 M. Anjomshoa, M. Torkzadeh-Mahani, J. Janczak, C. Rizzoli, M. Sahihi, F. Ataei and M. Dehkhodaei, Synthesis, crystal structure and Hirshfeld surface analysis of copper (II) complexes: DNA-and BSA-binding, molecular modeling, cell imaging and cytotoxicity, *Polyhedron*, 2016, **119**, 23–38.
60 A. Kosiha, C. Parthiban, S. Ciattini, L. Chelazzi and K. P. Elango, Metal complexes of naphthoquinone based ligand: synthesis, characterization, protein binding, DNA binding/cleavage and cytotoxicity studies, *J. Biomol. Struct. Dyn.*, 2018, **36**, 4170–4181.
61 P. Nariya, F. Shukla, H. Vyas, R. Devkar and S. Thakore, Synthesis, characterization, DNA/BSA binding and cytotoxicity studies of Mononuclear Cu(II) and V(IV) complexes of Mannich bases derived from Lawsone, *J. Mol. Struct.*, 2022, **1248**, 131508.
62 F. Abyar and L. Tabrizi, Experimental and theoretical investigations of novel oxidovanadium(IV) juglone complex: DNA/HSA interaction and cytotoxic activity, *J. Biomol. Struct. Dyn.*, 2020, **38**, 474–487.
63 A. Kosiha, C. Parthiban and K. P. Elango, Metal(II) complexes of bioactive aminonaphthoquinone-based ligand: synthesis, characterization and BSA binding, DNA binding/cleavage, and cytotoxicity studies, *J. Coord. Chem.*, 2018, **71**, 1560–1574.
64 P. Krishnamoorthy, P. Sathyadevi, A. H. Cowley, R. R. Butorac and N. Dharmaraj, Evaluation of DNA binding, DNA cleavage, protein binding and *in vitro* cytotoxic activities of bivalent transition metal hydrazone complexes, *Eur. J. Med. Chem.*, 2011, **46**, 3376–3387.
65 M. R. Eftink, Intrinsic Fluorescence of Proteins, in *Topics in Fluorescence Spectroscopy: Volume 6: Protein Fluorescence*, ed. J. R. Lakowicz, Springer, US, Boston, MA, 2000, pp. 1–15.
66 M. Anjomshoa, S. J. Fatemi, M. Torkzadeh-Mahani and H. Hadadzadeh, DNA- and BSA-binding studies and anticancer activity against human breast cancer cells (MCF-7) of the zinc(II) complex coordinated by 5,6-diphenyl-3-(2-pyridyl)-1,2,4-triazine, *Spectrochim. Acta, Part A*, 2014, **127**, 511–520.
67 K. Sakthikumar, R. V. Solomon and J. D. Raja, Spectro-electrochemical assessments of DNA/BSA interactions, cytotoxicity, radical scavenging and pharmacological implications of biosensitive and biologically active morpholine-based metal(ii) complexes: a combined experimental and computational investigation, *RSC Adv.*, 2019, **9**, 14220–14241.
68 J. R. Lakowicz and G. Weber, Quenching of protein fluorescence by oxygen. Detection of structural fluctuations in proteins on the nanosecond time scale, *Biochemistry*, 1973, **12**, 4171–4179.
69 W. Kaim, B. Schwederski and A. Klein, *Bioinorganic Chemistry-Inorganic Elements in the Chemistry of Life: an Introduction and Guide*, John Wiley & Sons, 2013.
70 U. Ndagi, N. Mhlongo and M. E. Soliman, Metal complexes in cancer therapy - an update from drug design perspective, *Drug Des. Dev. Ther.*, 2017, **11**, 599–616.
71 A. Pasini and F. Zunino, New cisplatin analogues—on the way to better antitumor agents, *Angew Chem. Int. Ed. Engl.*, 1987, **26**, 615–624.
72 P. M. Herst, T. Petersen, P. Jerram, J. Baty and M. V. Berridge, The antiproliferative effects of phenoxodiol are associated with inhibition of plasma membrane electron transport in tumour cell lines and primary immune cells, *Biochem. Pharmacol.*, 2007, **74**, 1587–1595.
73 W. Mahavorasirikul, V. Viyanant, W. Chaijaroenkul, A. Itharat and K. Na-Bangchang, Cytotoxic activity of Thai medicinal plants against human cholangiocarcinoma, laryngeal and hepatocarcinoma cells in vitro, *BMC Compl. Alternative Med.*, 2010, **10**, 55.
74 Y. Tian, H. Qi, G. Wang, L. Li and D. Zhou, Anticancer effect of sodium metavanadate on murine breast cancer both *in vitro* and *in vivo*, *BioMetals*, 2021, **34**, 557–571.
75 S. Kumar, S. Kumari, R. Karan, A. Kumar, R. K. Rawal and P. Kumar Gupta, Anticancer perspectives of vanadium complexes, *Inorg. Chem. Commun.*, 2024, **161**, 112014.
76 L.-P. Lu, F.-Z. Suo, Y.-L. Feng, L.-L. Song, Y. Li, Y.-J. Li and K.-T. Wang, Synthesis and biological evaluation of vanadium complexes as novel anti-tumor agents, *Eur. J. Med. Chem.*, 2019, **176**, 1–10.
77 D. Rehder, The role of vanadium in biology, *Metallomics*, 2015, **7**, 730–742.
78 P. Zhang and P. J. Sadler, Redox-active metal complexes for anticancer therapy, *Eur. J. Inorg. Chem.*, 2017, **2017**, 1541–1548.
79 T. Scior, J. Antonio Guevara-Garcia, Q.-T. Do, P. Bernard and S. Laufer, Why antidiabetic vanadium complexes are not in the pipeline of "big pharma" drug research? A critical review, *Curr. Med. Chem.*, 2016, **23**, 2874–2891.
80 S. P. Dash, A. K. Panda, S. Pasayat, S. Majumder, A. Biswas, W. Kaminsky, S. Mukhopadhyay, S. K. Bhutia and R. Dinda, Evaluation of the cell cytotoxicity and DNA/BSA binding and cleavage activity of some dioxidovanadium (V) complexes containing aroylhydrazones, *J. Inorg. Biochem.*, 2015, **144**, 1–12.
81 M. T. Islam, M. N. A. Bitu, M. A. Ali, M. F. Hossen and M. Kudrat, *Oxovanadium (IV) Complexes of α-Amino Acid Schiff Bases and 2, 2′-Bipyridine Ligands: Synthesis, Characterization and Investigation of Their Biological Potency*, 2024.
82 C. J. Weydert and J. J. Cullen, Measurement of superoxide dismutase, catalase and glutathione peroxidase in cultured cells and tissue, *Nat. Protoc.*, 2010, **5**, 51–66.
83 M. Turtoi, M. Anghelache, A. A. Patrascu, C. Maxim, I. Manduteanu, M. Calin and D.-L. Popescu, Synthesis, Characterization, and *In Vitro* Insulin-Mimetic Activity Evaluation of Valine Schiff Base Coordination Compounds of Oxidovanadium(V), *Biomedicines*, 2021, **9**, 562.
84 M. K. Mishra, R. Tripathi, P. Kb and T. Ip, α-amylase inhibition and electrochemical behaviour of some

oxovanadium (IV) complexes of l-amino acids, *Asian J. Pharm. Clin. Res.*, 2018, **11**, 218–224.

85 M. A. Hasan, H. Rahman, M. M. Haque and M. N. Islam, Synthesis, Characterization and In-vitro Antibacterial Activity Studies of Oxovanadium (IV) Complexes of α-Amino Acid Schiff Bases and 1, 10-Phenanthroline Ligands, *Asian J. Chem. Sci.*, 2024, **14**, 68–82.

86 H.-Y. Qian, Synthesis, Characterization, X-Ray Crystal Structures and Antibacterial Activities of Oxidovanadium (V) Complexes with Hydrazone and Hydroxamate Ligands, *Acta Chim. Slov.*, 2019, **66**, 995.

87 E.-C. Liu, W. Li and X.-S. Cheng, Synthesis, Spectroscopic Characterization, Crystal Structures and Antibacterial Activity of Vanadium (V) Complexes of Fluoro-and Chloro-Substituted Benzohydrazone Ligands, *Acta Chim. Slov.*, 2019, **66**, 971.